LUND UNIVERSITY

Physicochemical properties and atmospheric ageing of soot - investigated though aerosol mass spectrometry

Eriksson, Axel

2015

Link to publication

Citation for published version (APA):
Eriksson, A. (2015). *Physicochemical properties and atmospheric ageing of soot - investigated though aerosol mass spectrometry*. [Doktorsavhandling (monografi)].

Total number of authors:
1

General rights
Unless other specific re-use rights are stated the following general rights apply:
Copyright and moral rights for the publications made accessible in the public portal are retained by the authors and/or other copyright owners and it is a condition of accessing publications that users recognise and abide by the legal requirements associated with these rights.
• Users may download and print one copy of any publication from the public portal for the purpose of private study or research.
• You may not further distribute the material or use it for any profit-making activity or commercial gain
• You may freely distribute the URL identifying the publication in the public portal

Read more about Creative commons licenses: https://creativecommons.org/licenses/

Take down policy
If you believe that this document breaches copyright please contact us providing details, and we will remove access to the work immediately and investigate your claim.

LUND UNIVERSITY

PO Box 117
221 00 Lund
+46 46-222 00 00

Physicochemical properties and atmospheric ageing of soot

Investigated through aerosol mass spectrometry

Axel Eriksson

LUND
UNIVERSITY

DOCTORAL DISSERTATION
by due permission of the Faculty of Engineering, Lund University, Sweden.

To be defended in the Rydberg Hall, Physics Department, Professorsgatan 1, Lund.
June 12, 2015, 10.15.

Faculty opponent

Dr. Jay Slowik, Gasphase and Aerosol Chemistry Group,

Paul Scherrer Institute, Villigen, Switzerland

Organization: LUND UNIVERSITY

Physics Department, Nuclear Physics Division.

Author: Axel Eriksson

Document name: Doctoral thesis

Date of issue: 2015-05-19

Title and subtitle:

Physicochemical properties and atmospheric ageing processes of soot —Investigated through aerosol mass spectrometry

Aerosol particles contribute significantly to the global burden of disease, and remain the main source of uncertainty in assessments of human-induced climate change. The microphysical characterization of particles is necessary to understand the roles they play in the detrimental effects of air pollution on human health, and in the energy budget of our planet. Soot particles are especially relevant for climate and health, but the main component of soot – black carbon – is uniquely challenging to characterize. To meet this challenge, I have deployed a Soot-Particle Aerosol Mass Spectrometer (SP-AMS) to elucidate the physicochemical properties and atmospheric ageing processes of soot particles. The sources under investigation were appliances for residential heating, and light-duty vehicles.

Wood combustion emissions of particulate polyaromatic hydrocarbons (PAHs) are strongly dependent on combustion intensity: intense combustion results in oxygen deficiency in the appliance, which favors PAH emission. While most (>90%) of the particulate PAH mass was C24 or smaller, the observed distributions continued up to C48, with exponentially decreasing abundances. Excessively intense combustion also results in elevated emissions of secondary organic aerosol (SOA) precursors and soot. Contrary to expectations, the absorption Ångström exponent of the soot emitted was found to be fairly insensitive to photochemical processing, and similar to that of diesel exhaust particles.

Exhausts from gasoline powered light-duty vehicles were shown to readily form secondary organic aerosol (SOA). Roughly half of the SOA mass formed could be explained from reaction products of C6-C9 aromatics, which are known SOA precursors. The SOA had a similar elemental composition, volatility and density as the SOA formed by such precursors alone. The diesel exhaust particles were found to exhibit progressively enhanced hygroscopicity with photochemical processing due to the condensation of water-soluble material. The process of SOA condensation induced irreversible soot restructuring which was substantially accelerated by water uptake under humid (RH90) conditions.

The diesel particles observed in urban air were similar to the particles investigated in the laboratory in terms of size, shape, and mass spectral signature. Pure carbon ions as well as ions containing carbon and oxygen were unambiguously assigned to the refractory soot cores, in both laboratory and ambient air. In roughly five hours, highly aspherical, lightly coated, and hydrophobic fresh diesel exhaust particles were found to have aged into near spherical, more coated, and by inference hygroscopic accumulation mode particles. The transformation occurred under cold and humid conditions, despite limited photochemistry. Coupled ammonium nitrate and liquid water condensation was identified as the main cause of the transformation.

The processes controlling soot emission and transformation are elusive. Understanding has been impeded, despite considerable attention from the scientific community, by two inherent soot properties: stability and irregular shape. The same properties were exploited here, using state-of-the-art instrumentation to measure the physicochemical properties and atmospheric transformation of soot particles.

Key words: Black carbon, soot, vehicle exhausts, wood stove emissions, atmospheric processing, SP-AMS

ISSN and key title

Recipient's notes

ISBN 978-91-7623-369-6

Number of pages 157

Price

I, the undersigned, being the copyright owner of the abstract of the above-mentioned dissertation, hereby grant to all reference sources permission to publish and disseminate the abstract of the above-mentioned dissertation.

Signature Axel Eriksson Date 2015-05-04

Physicochemical properties and atmospheric ageing of soot

Investigated through aerosol mass spectrometry

Axel Eriksson

LUND
UNIVERSITY

Copyright Axel Eriksson

Faculty of Engineering, Physics Department, Nuclear Physics Division
ISBN 978-91-7623-369-6 (print)
ISBN 978-91-7623-370-2 (pdf)
Printed in Sweden by Media-Tryck, Lund University
Lund 2015

Tillägnas Sanna och Boya

Contents

Articles included in this thesis

I) **Eriksson, A.C.**, Nordin, E.Z., Nyström, R., Pettersson, E., Swietlicki, E., Bergvall, C., Westerholm, R., Boman, C., Pagels, J.H. (2014). Particulate PAH emissions from residential biomass combustion: time-resolved analysis with aerosol mass spectrometry. *Environmental Science and Technology*, 48(12), 7143-7150, doi: 10.1021/es500486j

II) Martinsson, J., **Eriksson, A.C.**, Elbæk Nielsen, I., Berg Malmborg, V., Ahlberg, E., Lindgren, R., Nyström, R., Nordin, E.Z., Brune, W., Svenningsson, B., Swietlicki, E., Boman, C., Pagels, J.H. Impacts of combustion conditions and photochemical processing on the light absorption properties of biomass combustion aerosol. Manuscript in preparation.

III) Nordin, E.Z., **Eriksson, A.C.**, Roldin, P., Nilsson, P.T., Carlsson, J.E., Kajos, M.K., Hellén, H., Wittbom, C., Rissler, J., Löndahl, J., Swietlicki, E., Svenningsson, B., Bohgard, M., Kulmala, M., Hallquist, M., Pagels, J.H. (2013). Secondary organic aerosol formation from idling gasoline passenger vehicle emissions investigated in a smog chamber. *Atmospheric Chemistry and Physics*, 13, 6101-6116, doi: 10.5194/acp-13-6101-2013

IV) Wittbom, C., **Eriksson, A.C.**, Rissler, J., Carlsson, J.E., Roldin, P., Nordin, E.Z., Nilsson, P.T., Swietlicki, E., Pagels, J.H., Svenningsson, B. (2014). Cloud droplet activity changes of soot aerosol upon smog chamber ageing. *Atmospheric Chemistry and Physics*, 14, 9831–9854, doi: 10.5194/acp-14-9831-2014

V) **Eriksson, A.C.**, Pagels, J.H., Wittbom, C., Sporre, M., Hermansson, E., Roldin, P., Nilsson, P., Martinsson, J., Rissler, J., Nordin, E.Z., Svenningsson, B., Swietlicki, E. Rapid atmospheric transformation of diesel soot particles despite limited photochemistry. Manuscript in preparation.

Author's contributions to the articles included in the thesis

I) I operated the Aerosol Mass Spectrometer which was the main instrument employed in this study and I analyzed and interpreted the resulting data. I developed the methodology used to infer emissions and heat output. I wrote the bulk of the text and designed and implemented many of the figures.

II) I conducted many of the Aethalometer and Soot-Particle Aerosol Mass Spectrometer measurements on which the paper is based. When not present on-site, I provided remote assistance to the operator. I devised the metric for light absorbing particulate carbon emissions, and wrote part of the manuscript.

III) I operated the Aerosol Mass Spectrometer, which was the main instrument employed in this study, and I analyzed and interpreted the resulting data. I designed and implemented many of the figures. I wrote part of the manuscript.

IV) I operated the Soot-Particle Aerosol Mass Spectrometer and analyzed and interpreted the resulting data. I assisted the lead author in writing the manuscript.

V) It was my initiative to combine the results from the three experimental campaigns involving diesel exhaust particles into one manuscript, which I wrote. I operated the Soot-Particle Aerosol Mass Spectrometer, which was the main instrument employed in this study, and I analyzed and interpreted the resulting data. I designed and implemented the figures.

Peer-reviewed articles not included in this thesis

vi) Yli-Juuti, T., Zardini, A.A., **Eriksson, A.C.**, Hansen, A.M., Pagels, J.H., Swietlicki, E., Svenningsson, B., Glasius, M., Worsnop, D.R., Riipinen, I., Bilde, M. (2013). Volatility of organic aerosol: evaporation of ammonium sulfate/succinic acid aqueous solution droplets. *Environmental Science & Technology*, 47(21), 12123-12130, doi: 10.1021/es401233c.

vii) Roldin, P., **Eriksson, A.C.**, Nordin, E.Z., Hermansson, E., Mogensen, D., Rusanen, A., Boy, M., Swietlicki, E., Svenningsson, B., Pagels, J. (2014). Modeling non-equilibrium secondary organic aerosol formation and evaporation with the aerosol dynamics, gas- and particle-phase chemistry and kinetic multi-layer model ADCHAM. *Atmospheric Chemistry and Physics*, 14, 7953-7993, doi: 10.1021/es5000353

iix) Rissler, J., Nordin, E.Z., **Eriksson, A.C.**, Nilsson, P.T., Frosch, M., Sporre, M.K., Wierzbicka, A., Svenningsson, B., Löndahl, J., Messing, M.E., Sjögren, S., Hemmingsen, J.G., Loft, S., Pagels, J.H. and Swietlicki, E. (2014). Effective density and mixing state of aerosol particles in a near-traffic urban environment. *Environmental Science and Technology*, 48(11), 6300-6308, doi: 10.1021/es500486j

ix) Nilsson, P.T., Isaxon, C., **Eriksson, A.C.**, Messing, M.E., Ludvigsson, L., Rissler, J., Hedmer, M., Tinnerberg, H., Gudmundsson, A., Deppert, K., Bohgard, M., Pagels, J.H. (2013). Nano-objects emitted during maintenance of common particle generators: direct chemical characterization with aerosol mass spectrometry and implications for risk assessments. *Journal of Nanoparticle Research*, 15(11), Nov. doi: 10.1007/s11051-013-2052-0

x) Isaxon, C., Dierschke, K., Pagels, J.H., Wierzbicka, A., Gudmundsson, A., Löndahl, J., Hagerman, I., Berglund, M., Assarsson, E., Andersson, U.B., Jönsson, B.A.G., Nøjgaard, J.K., **Eriksson, A.**, Nielsen, J., Bohgard, M. (2013). Realistic indoor nano-aerosols for a human exposure facility. *Journal of Aerosol Science*, 60, 55-56, doi: 10.1016/j.aerosci.2013.02.003

xi) Wierzbicka, A., Nilsson, P.T., Rissler, J., Sallsten, G., Xuc, Y., Pagels, J.H., Albin, M., Österbergc, K., Strandberg, B., **Eriksson, A.**, Bohgard, M., Bergemalm-Rynell, K., Gudmundsson, A. (2014). Detailed diesel exhaust characteristics including particle surface area and lung deposited dose for better understanding of health effects in human chamber exposure studies. *Atmoshperic Environment*, 86 212-219, doi: 10.1016/j.atmosenv.2013.11.025

xii) Nordin, E.Z., Uski, O., Nyström, R., Jalava, P., **Eriksson, A.C.**, Genberg, J., Roldin, P., Bergvall, C., Westerholm, R., Jokiniemi, J., Pagels, J.H., Boman, C., Hirvonen, M.-R. (2015). Influence of ozone initiated processing on the toxicity of aerosol particles from small scale wood combustion. *Atmoshperic Environment*, 102(0), 282-289, doi: 10.1016/j.atmosenv.2014.11.068

xiii) Roldin, P., Swietlicki, E., Massling, A., Kristensson, A., Londahl, J.L., **Eriksson, A.**, Pagels, J., Gustafsson, S. (2011). Aerosol ageing in an urban plume – implication for climate. *Atmospheric Chemistry and Physics*, 11(12), 5897-5915, doi:10.5194/acp-11-5897-2011

xiv) Crippa, M., Canonaco, F., Lanz, V., Äijälä, M., Allan, J., Carbone, S., Dall'Osto, M., Day, D.A., DeCarlo, P.F., Ehn, M., **Eriksson, A.**, Freney, E., Hildebrandt, L., Hillamo, R., Jimenez, J.-L., Junninen, H., Kiendler-Scharr, A., Kortelainen, A.-M., Kulmala, M., Mensah, A.A., Mohr, C., Nemitz, E., Ovadnevaite, J., Pandis, S., Petäjä, T., Poulain, L., Saarikoski, S., Sellegri, K., Swietlicki, E., Tiitta, P., Worsnop, D., Baltensperger, U., Prévôt, A.S.H. (2013). Organic aerosol components derived from 25 AMS datasets across Europe using a newly developed ME-2 based source apportionment strategy. *Atmospheric Chemistry and Physics*, 13(9), 23325-23371, doi: 10.5194/acpd-13-23325-2013

Symbols and abbreviations

λ	Wavelength
σ	Standard deviation
ω	Angular velocity
AAE	Absorption Ångström Exponent
AB	Air beam
ACI	Aerosol-cloud interaction
AMS	Aerosol Mass Spectrometer
APM	Aerosol Particle Mass analyzer
ARI	Aerosol-radiation interactions
BC	Black carbon, see “Soot and related terms”
BrC	Brown carbon
C	Species mass concentration
CCN	Cloud condensation nuclei
CE	Collection efficiency
CPC	Condensation Particle Counter
D^*	Characteristic particle diameter
D_a	Aerodynamic diameter
D_{va}	Vacuum aerodynamic diameter
D_z	Mobility diameter
DMA	Differential Mobility Analyzer
DSF	Dynamic shape factor
E_B	Particle bounce component of CE
E_L	Lens transmission component of CE
E_S	Beam divergence component of CE

EI	Electron ionization
ERF	Effective radiative forcing
HGF	Hygroscopic growth factor
HR	High resolution
I	Ion rate
IR	Infrared
IToF	Ion Time-of-Flight
LAC	Light absorbing carbon
m/z	Ion mass to charge ratio
mIE	Mass specific ionization efficiency
m_p	Particle mass
nR-PM	Non-refractory PM
OA	Organic aerosol
OS_C	Average carbon oxidation state
PAM	Potential Aerosol Mass chamber
PAH	Polyaromatic hydrocarbon
POA	Primary organic aerosol
PM	Particulate matter
PM_x	Volumetric mass concentration of PM with D_a < x μm
PSL	Polystyrene latex
PToF	Particle Time-of-Flight
r	Radius
rBC	Refractory black carbon, see “Soot and related terms”
$rC_xH_y^+$	Carbon and hydrogen containing ions from rBC
$rC_xO_y^+$	Carbon and oxygen containing ions from rBC
Q	Volumetric sampling flow rate
q_p	Particle charge
RF	Radiative forcing
RIE	Relative ionization efficiency
SLCF	Short-lived climate forcer

SMPS	Scanning Mobility Particle Sizer
SOA	Secondary organic aerosol
SP2	Singe-Particle Soot Photometer
SP-AMS	Soot-Particle Aerosol Mass Spectrometer
PSAP	Particle Soot Absorption Photometer
U	Voltage
UMR	Unit mass resolution
UV	Ultraviolet
v_g	Gas velocity after expansion
v_l	Gas velocity in lens
v_p	Particle velocity

Soot and related terms

In addition to being uniquely interesting, and important with regards to climate forcing and adverse health effects, soot particles are also uniquely confusing. This due in part to the alternating terms in the literature that denote the same thing (the same thing has different names), and to the inconsistent usages of these terms (the same name refers to different things). Petzold and et al.[1] have attempted to mitigate this issue though suggestions on terminology. These suggestions have been followed in this research. The key terms are summarized and discussed below.

Soot: Carbonaceous particles formed from incomplete combustion. Refers to the entire particle as it occurs on emission, without reference to specific properties (other than carbonaceous), or the means of detection. A particle that has grown by condensation onto a soot particle, or that has had soot particles impacted on it, is referred to as a **soot containing particle**. I believe soot has the advantage of being a generally accessible term, as it is part of the vocabulary of many non-specialists. It is also commonly used in the combustion science community in contexts where some of the subtleties required in environmental sciences are redundant (e.g., there is no need to specify whether nonexistent organic coatings are included in the particle in-flame). By **atmospheric ageing of soot** I mean the processes which determine the evolving properties of the soot and soot containing particles in the atmosphere.

Black carbon (BC): A qualitative description referring to materials that share the following five properties: strong light absorption (>5 m^2/g at 550 nm), graphite-like structure (a large fraction of sp^2 bonded carbon), thermal stability (volatilization

temperature near 4000 K), insolubility in water or other solvents, and fractal like morphology which consists of agglomerates of tens to hundreds of spherules between <10 nm and ~50 nm. It is customary to refer to these spherules as **primary particles**. Because the term "primary particles" is also used to describe PM which emitted, as opposed to formed in the atmosphere (called secondary, see section 2.1), which is true of the agglomerates as well, the small spherules will henceforth be refed to as **BC monomers** (also frequently used in the literature) instead. This has the added value of emphasizing that the BC (agglomerate) particle consists of smaller sub-units.

Refractory black carbon (rBC): Black carbon as measured by the Soot Particle Aerosol Mass Spectrometer (SP-AMS). The salient feature of the article by Petzold et al.[1] is that when measurements are discussed, the word used to describe the measured black carbon (or black carbon containing) particles should reflect the technique used. For SP-AMS data, the term rBC is used because both thermal stability and light absorption are used (see section 3.1.1) to detect the particles.

Light absorbing carbon (LAC): Optically defined quantity, determined through light absorption (the unit is m^{-1}). In the research presented here, LAC was measured by means of filter deposition at seven wavelengths (see section 3.2.4). The LAC measured at each wavelength was operationally divided into "black" and "brown" carbon (BrC) by postulating that only BC absorbs infrared light, and that BC absorption can be extrapolated from the infrared to ultraviolet using the absorption Ångström exponent (AAE) 1.

Populärvetenskaplig sammanfattning

Sotpartiklar i atmosfären är en del av klimatfrågan som är i särskilt stort behov av utredning. Dessutom har det visat sig, att samma partiklar orsakar mycket stora hälsoproblem; globalt, på Europeisk nivå, och till och med i förhållandevis förskonade länder som Sverige.

Vi vet nu nästintill helt säkert att mänsklig påverkan leder oss in i ett varmare klimat. Vi behöver bättre förstå hur, och hur fort, för att kunna hitta de bästa lösningarna. Luftburna partiklars påverkan på klimatet är den största källan till osäkerheter, och sot är den viktigaste, men samtidigt mest komplicerade partikeltypen. Många partiklar har naturligt ursprung: de är inte ett resultat av mänskliga aktiviteter. Sotpartiklar däremot kommer i stor utsträckning från utsläpp orsakade av människor. I Europa kommer de flesta sotpartiklar från dieselmotorer och vedeldning, det är de partiklarna som jag har studerat i denna avhandling.

De flesta partikeltyper bidrar till att bromsa klimatförändringarna genom att reflektera tillbaka solljus till rymden. Sotpartiklarna har ju den utmärkande egenskapen att de är svarta, och gör därför istället problemet värre genom att effektivt absorbera solljus. Molnbildning är en mycket viktig del av partiklarnas roll i klimatet. Framförallt sprider molndroppar, likt partiklar, solljus tillbaka till rymden; de bromsar klimatförändringarna. Moln, och i förlängningen regn, är ju också viktigt för annat än klimatförändringar! Varje molndroppe har från början varit en partikel: utan partiklar, blir det inga moln. Det är dock inte alla partiklar som kan bilda molndroppar.

Våra experiment visar till exempel att sot som nyligen släppts ut av dieselbilar inte alls bildar molndroppar i atmosfären. När utsläppen bestrålas med UV-ljus förändras dock sotpartiklarnas egenskaper, och de kommer därför att börja påverka molnbildning efterhand. Det beror på att organiska föreningar bildas, som kondenserar på sotet. Vi har också visat att avgaser från bensinbilar är en effektiv källa till sådana organiska föreningar. När de organiska föreningarna kondenserar på sotet förändras dess karaktär helt. Det färska sotet består av spretiga agglomerat som vatten inte kan kondensera på. Den organiska beläggningen bidrar förutom till att sotpartikeln kan ta upp vatten, också till att dess form ändras. Man vet inte med säkerhet vilken roll formen spelar för sotpartiklars roll i klimatförändringar, eller för deras hälsoeffekter, men det finns skäl att tro att formen är viktig till exempel för ljusabsorption.

Vi har också kommit fram till, att dieselsot ändrar karaktär oväntat fort i atmosfären. Vi mätte vintertid sotpartiklar vid en gata i centrala Köpenhamn, och på Söderåsen, cirka sex mil därifrån fågelvägen. Sedan valde vi ut tidpunkter då luften på Söderåsen hade passerat över Köpenhamn. Vi kunde därefter sluta oss till att de partiklar som cirka fem timmar tidigare när de släppts ut i Köpenhamn varit helt färska, hade transformerats till åldrade partiklar under transporten över sundet. Detta var en oväntad upptäckt eftersom det fanns begränsat med UV-ljus, som normalt är själva drivkraften för transformationen. Vi har kommit fram till att det var samverkan mellan oorganiska föreningar och vatten som åstadkom den snabba transformationen.

Våra studier av vedrök visar att det är väldigt viktigt för utsläppen hur eldningen sköts. Våra mätningar visar att när det brinner för intensivt i en vedkamin, ökar utsläppen av klimat- och hälsopåverkade partiklar. Det är ju tydligt för envar att för långsam eldning, där veden ligger och pyr, är dåligt. Det våra resultat visar är att motsatsen: för intensiv, snabb eldning, leder till andra typer av utsläpp. De utsläppen kan ha minst lika stor påverkan på hälsa och klimat, men är mindre uppenbara. Mycket av partikelmassan från sådan eldning bildas till exempel efter att utsläppen åldrats flera dagar i atmosfären!

En av anledningarna till att just sotpartiklar är så komplicerade att reda ut är att det är svårt att mäta deras egenskaper. Till både form och innehåll skiljer de sig nämligen från de flesta av de luftburna partiklarna. De består till stor del av grafitliknande material som inte enkelt går att lösa upp, och kräver mycket höga temperaturer för att förånga. Luftburna partiklar i allmänhet är en utmaning för mättekniken: de väger tillsammans normalt sett mindre än en tiondels miljondel av luften som bär upp dem. Om man samlar in partiklarna på ett filter påverkar man ofta egenskaperna som mäts. Därför har jag använt ett nyligen utvecklat mätinstrument: sotpartikel-aerosolmasspektrometer (SPAMS). SPAMSen förångar sotpartiklarna utan filterinsamling med hjälp av en kraftfull laser, och sedan analyseras ångorna. Eftersom analysen sker i princip i realtid går det att följa snabba förlopp som vedeldning. Ingen av studierna i avhandlingen hade varit möjlig utan SPAMS.

1. Background

1.1 Why study aerosols? Why focus on soot particles? Why use aerosol mass spectrometry?

Aerosol particles are strongly linked to the global burden of disease and human-induced climate change – the latter of which is arguably the main challenge our species is currently facing. But aerosol particles have also been central in shaping our world. Without them there would be no clouds on planet Earth, and consequently no rain. Aerosol particles from volcanic eruptions and/or asteroid impacts are also the main suspects in what caused the mass extinctions that set the stage for life on Earth as we know it today. The World Health Organization (WHO) attributes one eighth of the deaths which occured in the year 2012 to air pollution[2]. Aerosol particles are known to play a major role in health outcomes from air pollution. The Intergovernmental Panel on Climate Change (IPCC) recently assessed that "clouds and aerosols continue to contribute the largest uncertainty to estimates and interpretations of the Earth's changing energy budget"[3]. Hence, there are good reasons to study aerosol particles: to attain a fundamental understanding of the Earth system, and to mitigate major societal problems.

There are two features that make soot uniquely interesting among aerosol particles. The first is that soot particles, and soot-containing particles, are very efficient light absorbers. They absorb sunlight which would otherwise have been reflected back into space. This affects the accumulation and distribution of heat in the Earth system. The second feature is that the characteristic length scale of soot is very small, even compared with other aerosol particles: tens of nanometers. In contrast to many other particle constituents, this scale does not change in the atmosphere. The soot part of a particle will neither grow nor shrink after emission (several particles can coagulate into a bigger one, but they are still separate). Small things have large surfaces, in relation to their mass, and soot particles can have more than 100 square meters surface area per gram[4]. Many interesting and important things happen at surfaces: gases are adsorbed and chemical reactions are catalyzed.

The use of in-situ aerosol mass spectrometry[5, 6] has revolutionized our understanding of organic aerosols[7]. That is because an aerosol is a very dilute and dynamic system. When concentrated, collected and transported for subsequent analysis elsewhere, the

system is perturbed and will evolve in ways which are not always readily accounted for. In addition to organic and inorganic (non-carbonaceous) aerosol particle constituents, the aerosol mass spectrometry technique was recently improved to include soot[8]. It remains to be seen what we will learn about soot as a consequence, but the research presented in this thesis features some early applications of this expanded technique: the Soot-Particle Aerosol Mass Spectrometer.

I have used the recently developed Soot-Particle Aerosol Mass Spectrometer to investigate two of the main sources of soot particles: residential biomass combustion and diesel-powered vehicles. Laboratory experiments were performed which simulated the atmospheric ageing of soot particles under controlled conditions. Ambient measurements were also carried out that show how soot particles can transform in the atmosphere after emission.

1.2 Aim and objectives

The aim of the research presented was to elucidate the processes that govern the emission and atmospheric ageing of soot particles. These processes determine particles' physicochemical properties, which in turn determine their impacts on the Earth's climate, and on human health. In order to quantify the impacts of soot emissions, models are needed which adequately describe the particles: models which originate from and are validated by empirical observations. My objective has been to make and interpret such observations, specifically pertaining to:

I) The influence of wood combustion conditions on the amount and properties of the primary particles emitted, and secondary materials formed from the emissions after atmospheric ageing.

II) The initial (hours-days) atmospheric ageing of light-duty vehicle emissions, especially diesel soot: under controlled conditions in the laboratory, and in ambient air.

2. Introduction

> "A working party is, however, and in strict accordance with Government policy, considering legislation to compel those in Fresh Air Surplus areas into wearing gas masks connected to bottles of potted smog."
>
> From the short story, "Kindly Breathe in Short, Thick Pants" about Britain's fictional 1976 fresh air crisis, by Terry Prachett (1948-2015), in *A Blink of the Screen: Collected Short Fiction*, 2012, p. 62.

The Earth's atmosphere contains suspended particulate matter (PM). This matter is ubiquitous, but varies considerably in its properties, both intrinsically and with regards to concentration. However, the particles are clearly (at least conceptually) separated from the bulk of the atmosphere's mass by a difference in phase: particles being liquid, solid or in-between. The term "aerosol" refers to such suspended particles and the gases which carry them collectively. (This definition is generally agreed upon by those who work in the field; however, many scholars use the word "aerosol" to denote the particles in isolation, causing irritation and to a lesser extent ambiguity.)

While it has long been known that some of these particles have an adverse effect on human health (e.g., miners suffering from respiratory diseases due to dust inhalation), the integrated impacts of atmospheric aerosol particles are still poorly bounded. This is partly due to a lack of understanding of the processes that form the particles and determine their physicochemical properties. In order to understand the effects of the particles, their properties have to be determined. Atmospheric transformation also changes the particle properties, exacerbating the complexity of determining their impacts.

Atmospheric particle abundances are often expressed in terms of volumetric number or mass concentration, both of which may vary by five orders of magnitude. Ambient number concentrations can range from a few particles to hundreds of thousands of particles per cm^3. The ambient mass concentration per m^3 ranges from nanograms to hundreds of micrograms. In terms of single particle size, there is also a big span: particle diameters range from a few nanometers, (below which the phase is ill-defined and the word "cluster" is typically used instead), to a few tens of micrometers, above which the gravitational settling will prevent extended periods of suspension. In terms of mass, that corresponds to a difference by twelve orders of magnitude: comparing

the smallest and largest particles is equivalent to comparing one chicken and hundreds of millions of elephants. When it comes to mass concentrations of particulate matter, which is the focus of this thesis, the abbreviation PM_x (where x is usually 1, 2.5 or 10) is used to indicate concentration of particles which have a diameter smaller than x μm.

2.1 Primary and secondary

A distinction often made is between primary and secondary PM. Primary PM is emitted directly, while secondary PM is formed in the atmosphere. There are three known pathways through which secondary PM is formed. The first is gas to particle conversion, when gas-phase chemical reactions form products of lower saturation vapor pressures, that partition into the condensed phase, either through new particle formation or through condensation onto pre-existing PM. Article III examines gas to particle conversion in exhausts from gasoline vehicles. The second is aqueous-phase secondary PM, which forms as gas phase precursors dissolve in water droplets and undergo chemistry that results in species which remain in the condensed phase as the water evaporates. Finally, there is heterogeneous formation, in which gas and condensed phase molecules react, yielding increased PM mass.

2.2 Climate effects

While there is now an overwhelming consensus among scholars that the climate is being perturbed by past and present anthropogenic activities[9], some aspects of the process are better understood than others. The fundamental issue is clear: the Earth system is continuously acquiring more heat as time passes. This is manifested as rising temperatures in the atmosphere and oceans, and reduced amounts of sea ice and glaciers. The cause is also largely undisputed: the balance between energy radiating into the Earth system and radiating out of it is shifting because of pollutants referred to as "climate forcers" (CF). The main CF is carbon dioxide released by the burning of fossil fuel. Carbon dioxide is a naturally occurring constituent of the atmosphere. It is the chemical form in which carbon, which is necessary for all life as we know it, mainly enters the biosphere through photosynthesis. It is also the main route through which carbon leaves the biosphere (sometimes dwelling in intermediate forms such as methane first), completing the cycle. The problem is that the cycle is skewed by the harvesting of fossil fuels. Carbon that has been accumulating as fossil fuel over millions of years is being released back into the atmosphere over timescales of centuries. Consequently, the concentration of carbon dioxide rises[10]. This affects the Earth's energy budget, because carbon dioxide absorbs the long wavelength radiation

emanating from the planet, while it is transparent to the short wavelength radiation received from the sun, henceforth referred to as "sunlight" for brevity.

Much of the research into atmospheric aerosols is aimed at understanding their climatic effects. That is because unlike carbon dioxide, PM interacts with the energy budget of the Earth in many, sometimes complicated ways. This is hardly surprising: carbon dioxide is carbon dioxide is carbon dioxide – a single, simple molecule. Its turnover time in the atmosphere is about a century, so it has time to mix and is found in approximately the same proportions everywhere. PM on the other hand, refers to anything which is lumped together in pieces between nanometers and micrometers in size and suspended in air for durations which vary from hours to months.

By reducing the flux of infrared radiation out of the earth system, without a similar reduction in incoming sunlight, excess carbon dioxide from fossil fuel burning induces radiative forcing (RF). Since this is a process which affects the energy budget of the entire Earth system, a metric often used to describe RF is globally averaged W/m^2. By convention, heating RF is assigned positive values. It should be noted that RF is a perturbation. This means that RF is the *difference* in radiative flux, not the flux itself. In order to establish the difference in flux, a reference is needed where the anthropogenic influence on the planet's radiative budget was small. The year 1750 is often taken as this reference.

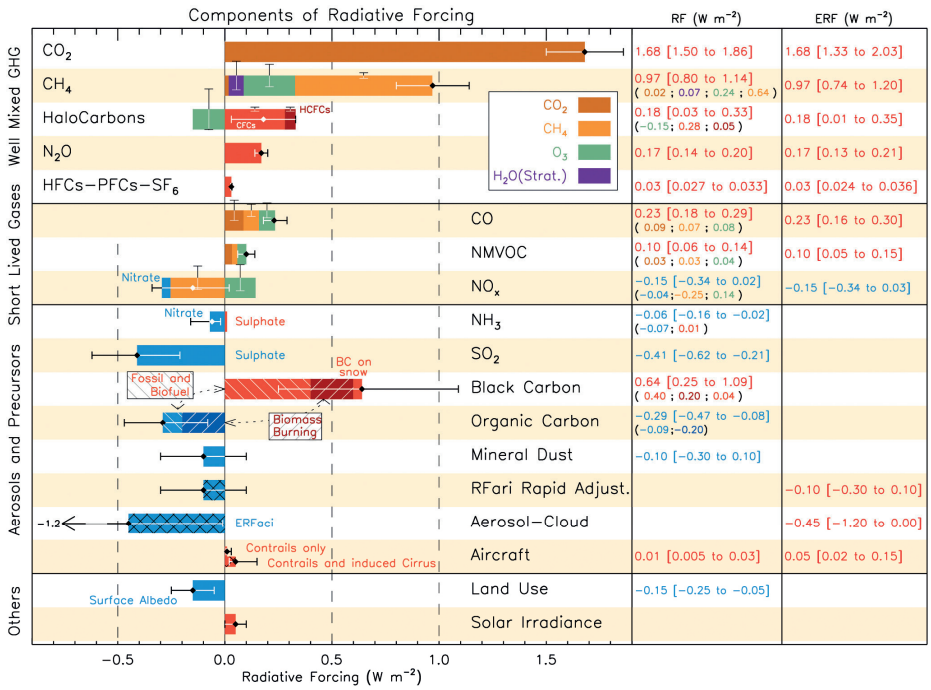

Figure 1. Radiative forcing (RF) from 1750 to 2011 by emitted components. Effective radiative forcing (ERF) quantifies the impact of rapid atmospheric adjustments. From Stocker and co-workers[11], 2013: *Figure TS.7 | Radiative forcing (RF) of climate change during the Industrial Era shown by emitted components from 1750 to 2011. The horizontal bars indicate the overall uncertainty,while the vertical bars are for the individual components (vertical bar lengths proportional to the relative uncertainty, with a total length equal to the bar width for a ±50%uncertainty). Best estimates for the totals and individual components (from left to right) of the response are given in the right column. Values are RF except for the effective radiative forcing (ERF) due to aerosol–cloud interactions (ERFaci) and rapid adjustment associated with the RF due to aerosol-radiation interaction (RFari Rapid Adjust.). Note that the total RF due to aerosol-radiation interaction (–0.35 Wm^{-2}) is slightly different from the sum of the RF of the individual components (–0.33 Wm^{-2}). The total RF due to aerosol-radiation interaction is the basis for Figure SPM.5. Secondary organic aerosol has not been included since the formation depends on a variety of factors not currently sufficiently quantified. The ERF of contrails includes contrail induced cirrus. Combining ERFaci –0.45 [–1.2 to 0.0] Wm^{-2} and rapid adjustment of ari –0.1 [–0.3 to +0.1] Wm^{-2} results in an integrated component of adjustment due to aerosols of –0.55 [–1.33 to –0.06] Wm^{-2}. CFCs = chlorofluorocarbons, HCFCs = hydrochlorofluorocarbons, HFCs = hydrofluorocarbons, PFCs =perfluorocarbons, NMVOC = Non-Methane Volatile Organic Compounds, BC = black carbon. Further detail regarding the related Figure SPM.5 is given in the TS Supplementary Material. Figure 8.17*

The ways in which aerosol particles perturb the climate can be divided into aerosol-radiation interactions (ARI) and aerosol-cloud interactions (ACI). ARI have previously been referred to as "direct", while ACI have been termed "indirect" effects of aerosol particles (to reflect the fact that the clouds in turn interact with radiation). ARI involve particle interactions with sunlight, while clouds interact with both sunlight and infrared radiation emitted by the Earth system.

Aerosol-radiation interactions come in two varieties: scattering and absorption. The particles impact our climate by scattering sunlight, partly away from the Earth, which leads to cooling. Some particles also absorb sunlight, which has the opposite effect. It adds to the accumulation of heat caused by excess carbon dioxide, which is driving the change towards a hotter climate.

Clouds are very important for the radiative balance of the earth system, mainly because they reflect sunlight, which causes cooling. Since the water vapor in the atmosphere would not condense without aerosol particles acting as nuclei, the amount and distribution of aerosol particles has a controlling effect on clouds. It should be pointed out that there are other aspects of perturbations of clouds, and by extension rain, than RF. In Article II we investigated diesel exhaust particles, which are emitted in great abundance globally, as potential cloud condensation nuclei.

Black carbon (BC) is a term used to denote a subcategory of PM which is very efficient at absorbing sunlight (see "Soot and related terms"). BC emissions are very problematic because atom by atom, BC induces much more RF than any other emissions. Although BC is a small fraction of the anthropogenic PM, it causes disproportionately large perturbations of the climate system. In fact, while most PM has a net cooling effect, BC contributes significantly to the warming caused by humans. BC emissions are strongly liked to energy production (just like the excess carbon dioxide from fossil fuel use), as can be seen from Figures 1 and 2. It has been suggested that BC is the second most important climate forcer, intermediate between carbon dioxide and methane[12, 13]. Others estimate that methane emissions cause more forcing than BC emissions[11]. At any rate, there is a consensus that anthropogenic BC emissions are a very potent climate forcer.

Because of the limited atmospheric lifetime of black carbon (BC) (on the order of a week) compared to carbon dioxide (a century), BC is considered a "short-lived climate forcer" (SLCF). Globally averaged RF does not capture the full impact of BC on the climate system, since additional effects (beyond the shift of global radiative balance) occur[13]. These effects include accelerated snow and ice melting rates in the Arctic, and possibly regional circulation and precipitation changes[13]. In addition to having worse consequences for the climate than the globally averaged RF implies, SLCF also offers better near-term mitigation possibilities: the reduction in emission more quickly translates into reduced concentrations.

One difficulty of assessing the climatic impacts of individual pollutants is that no source emits one pollutant exclusively. There is thus some controversy over the magnitude of potential climate benefits from policies aimed at the reduction of SLCF. The benefits could be overestimated[14], since policies aimed at reducing carbon dioxide emissions will also reduce emissions of SLCFs such as BC as a co-benefit. Considering BC-rich sources exclusively, a recent comprehensive assessment by Bond et al.[13] found the best estimate combined RF to be near zero due to the cooling effect of co-emitted species (see Figure 2). The authors suggest that BC-rich sources can still offer policy

makers air quality improvement possibilities that are neutral with respect to radiative forcing[13]. As elevated PM concentrations cause adverse effects on human health (see section 2.3), it is highly desirable to find ways to reduce anthropogenic PM without sacrificing the cooling effects (see Figure 1).

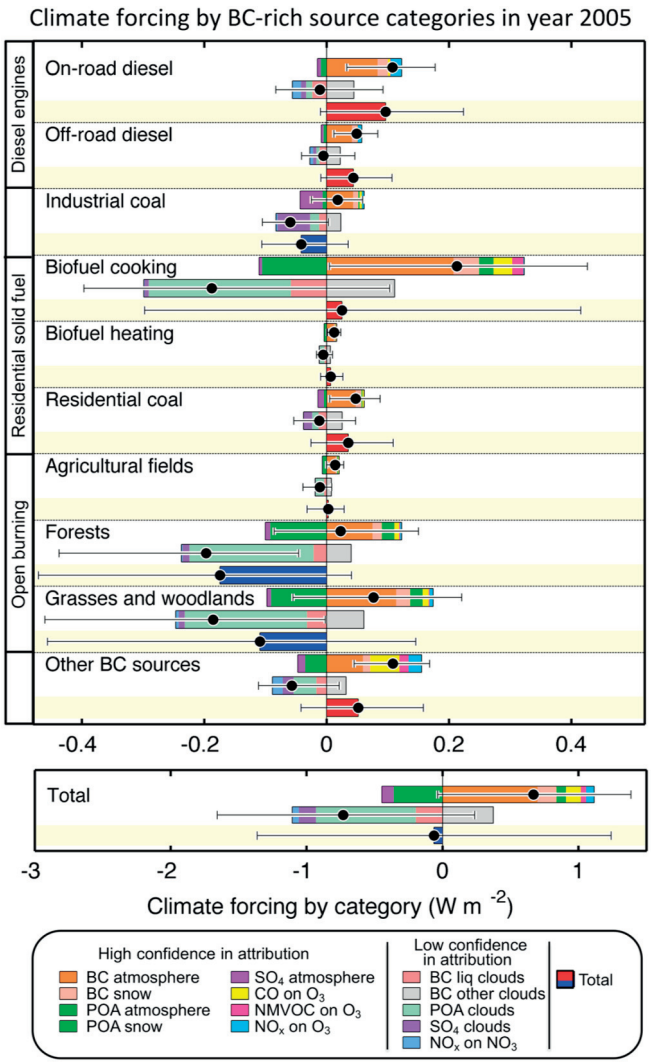

Figure 2. Climate forcing attributed to BC rich sources in 2005. Effects from each source category are grouped after confidence in attribution: high confidence (top), low confidence (middle), total (bottom). Figure 37 from Bond and co-workers[13], 2013.

Secondary organic aerosol (SOA, see section 2.1.1, and Articles II-V) is excluded from the assessments summarized in Figures 1 and 2. That is because the current understanding of the processes involved in SOA formation and evolution are

considered too tentative by the authors[11, 13]. While biogenic precursors are considered to dominate SOA globally, contributions from anthropogenic precursors are estimated to make non-negligible contributions as well[15]. Formation rates of SOA from anthropogenic precursors in the United States alone have recently been estimated as 0.7 Tg y^{-1}, most (estimated fraction 90%) of which was modelled as originating from biomass burning and gasoline vehicles[16]. Every aspect of BC-induced climate forcing (and, as recently reviewed by Bond et al[13], they are numerous) is affected by particle properties which evolve after emission. Atmospheric processing of combustion derived-PM precursor gases, and soot particles, clearly obscures our understanding of the consequences of their anthropogenic emissions.

2.3 Health effects

Particulate matter (PM) is known to cause adverse health effects. According to WHO, air pollution, of which PM is one of the main constituents, caused around 7 million deaths in 2012[2]. More than half of those deaths were attributed to indoor exposure, caused by residential use of solid fuels such as wood for cooking and heating purposes. Soot particles most probably played a major part in that outcome.

Epidemiological studies have shown that outdoor PM concentrations correlate with morbidity[17] and mortality[18]. Many studies suggest that the components in PM have different health outcomes[19]. Different particle sizes are commonly considered to have different toxicity: fine particles ($PM_{2.5}$) are often considered more detrimental to health than coarse particles (PM_{10}), on a mass basis[20]. That is because fine particles, also termed "respiratory particles", are able to penetrate deep into the human lung. Black carbon (BC) exposure has been found to more robustly predict adverse health outcomes than PM in general[21]. Toxicological studies suggest it is not the BC itself that causes the effects; rather, BC may act as a vector, transporting various toxins into the lungs[21]. However, implementing such PM differentiation in the assessment of the health outcomes has so far often been considered beyond state-of-the-art.

For instance, WHO currently recommends using the same mortality risk per $PM_{2.5}$ increase – 6.2% per 10 μg/m^3 – regardless of source and composition. Using these parametrizations, it was recently estimated that approximately 458 000 premature deaths were caused by air pollution in Europe in 2011[22]. This makes air pollution the leading environmental cause of premature death in Europe.

A recent assessment of the health impacts of air pollution in Sweden[20] has taken a less conservative approach and separates $PM_{2.5}$ into source specific impacts. Primary combustion generated particles (largely soot) from traffic and residential wood burning were considered roughly three times as toxic as other fine particles (17% increased mortality per 10 μg/m^3 compared with 6.2% per 10 μg/m^3). The estimated

death toll in the Swedish study was 5500 lives lost prematurely per year. Of that number, 3000 deaths were estimated to have been caused by non-local sources, 1000 from residential wood burning, and 1300 from vehicle exhaust (non-exhaust vehicle emissions account for 200).

While higher exposures are more detrimental to health, there does not seem to be a lower threshold below which PM does not cause adverse health effects[19]. Residential combustion of solid fuels, by the high indoor exposures they induce, causes by far the most harm to human health because roughly 3 billion people use such combustion on a daily basis[23]. In Europe, the aggregated costs (a large portion of which stems from health impacts from PM) of air pollution between 2008 and 2012 have been estimated to be in the range 329-1053 billion EUR_{2005} from industrial facilities alone[24]. In Sweden, despite comparatively low levels of air pollution, the estimated monetized value of the socio-economic cost of $PM_{2.5}$ in 2010 was 35 billion SEK_{2010}[20]. Taken together, the assessments of PM impacts on health on the global, European, and Swedish scales show that the problem is both massive and ubiquitous.

3. Method

The methods employed in this thesis are described and discussed below. Due to the interests and role of the author, experimental aspects of the research are treated exclusively, with focus on aerosol mass spectrometry. Table 1 summarizes the methods used in Articles I-V.

Table 1.
Overview of sources studied, campaigns performed and techniques employed in Articles I-V.

Article	I	II	III	IV	V
Source					
Wood smoke	x	x			
Vehicle exhaust			x	x	x
Campaign					
Laboratory	x	x	x	x	x
Ambient					x
Instrument					
AMS[a]	x	x	x	x	x
SP-AMS[b]		x	(x[c])	x	x
APM[d]				x	x
Ageing simulation					
Smog chamber			x	x	x
PAM[e]		x			

a Aerosol Mass Spectrometer, see section 3.1.
b Soot-Particle Aerosol Mass Spectrometer, see section 3.1.
c Features SP-AMS, but there was little soot, see section 4.2.1.
d Aerosol Particle Mass analyzer, see section 3.2.3
e Potential Aerosol Mass chamber, see section 3.2.2

3.1 Soot-Particle Aerosol Mass Spectrometer: SP-AMS

The Soot-Particle Aerosol Mass Spectrometer[8] (SP-AMS, Aerodyne) is an instrument that enables in-situ quantitative measurement of the time- and size-resolved chemical composition of PM_1. It consists of a High Resolution Time-of-Flight Aerosol Mass Spectrometer (HR-ToF-AMS[25], Aerodyne, henceforth: AMS) that has been equipped with a continuous wave IR laser (Nd:YAG 1064 nm). The latter was adapted from another instrument: the Single Particle Soot Photometer[26] (SP2, Droplet Measurement Technologies).

The AMS is a vacuum system with three main components: inlet, particle sizing chamber, and mass spectrometer.

The inlet consists of an orifice with a diameter of 0.1 mm, though which an aerosol flow of ~1.5 cm^3/s is sampled, followed by an aerodynamic lens. The lens, which consists of a series of concentric apertures, focuses particles into a collimated beam[27]. After passing a skimmer cone, the particle beam enters the sizing chamber.

In the particle sizing chamber the beam is modulated by means of a rotating "chopper" disc. The chopper periodically blocks the beam entirely, facilitating the measurement of instrumental background. In this manner, "closed" signal is acquired. The non-size resolved data (which is referred to as "MS" data) is obtained by subtracting the closed from "open" signal (acquired when the chopper is not blocking the beam). Size resolved data is acquired by positioning the chopper so that the particles are transmitted only through the two radial slits which together make up 2% of the circumference (i.e., as the chopper rotates, 98% of the particles are lost from the beam). Thus the chopper provides a well-defined start of the Particle Time-of-Flight (PToF) through the sizing chamber. The PToF, which ranges from 1 to 5 ms, is interpreted in terms of aerodynamic diameter, further discussed in section 3.1.2.2.

The particle beam is terminated by a heated (normally kept at 600 °C) tungsten vaporizer. Upon impaction, the operationally defined non-refractory particulate matter (nR-PM) flash vaporizes, which makes it eligible for mass spectrometric analysis. The vapors are subsequently ionized by means of 70 eV electron ionization (EI). The combined effects of flash vaporization and EI produces positively charged molecular fragments. The fragmentation is normally extensive, which means individual molecular abundances in complex orgaic mixtrures cannot be retrieved. Instead, the data are interpreted in terms of factor analysis[28] (where the complex mixture is deconvolved into subcategories) or by calculating average properties such as the carbon oxiation state[29]. Furthermore, the vapors are typically not assigned to individual particles: instead particle ensemble composition is measured.

The fragments are extracted into an Ion Time-of-Flight (IToF) chamber, where they are orthogonally pulsed into a V-shaped trajectory (the turn extends the flight path, and in addition narrows the IToF distribution of each ion type). The IToF, typically

ranging from 1 to 20 μs, is interpreted in terms of mass to charge ratio (m/z), further described in section 3.1.3.

3.1.1 Soot-Particle module

The usefulness of the AMS technique is its generality: most of PM_1 is in the non-refractory category and thus readily measured. Although previously thought unattainable, quantitative measurement of sea salts[30] and lead[31], as well as detection of several other trace elements[32] (which implies that quantification is possible), have also been demonstrated. There is however a very important exception from this generality – black carbon (BC, see "Soot and related terms"). As the vaporization temperature of BC is around 4000 K, it cannot be detected using the tungsten vaporizer.

In order to overcome this problem, a soot-particle module was recently added to the design[8]. The module consists of an intra-cavity 1064 nm Nd:YAG laser, which functions as a soot particle vaporizer. The laser beam heats absorbing species, such as BC and metals[33], until vaporization. BC as measured with the SP-AMS and similar techniques is referred to as "refractory black carbon" (rBC, see "Soot and related terms"). Other species that are internally mixed (i.e., present in the same particles) with the absorbing species evaporate as the particle heats. Owing to the high vaporization temperature of rBC, it can normally be assumed that everything which is internally mixed with rBC will be detected.

There are two possible configurations of the SP-AMS: single and dual vaporizer[8]. In the single vaporizer configuration, the tungsten vaporizer is removed from the instrument. This enables the selective detection of particles containing rBC (or other IR absorbing species). The single vaporizer configuration has two advantages. The first is that the selective detection of particles containing rBC enables the measurement of the particle mixing state: all non-rBC material detected was internally mixed with rBC, and therefore the rBC fraction of the particles can be calculated. The second advantage is that all the signals recorded originate from vapors generated using the same mechanism (the gradual heating of rBC-containing particles), which reduces the complexity of the measurement. The disadvantages of the single vaporizer configuration are that generality is lost (as non-absorbing particles will not be detected), and that the calibration procedures (see section 3.1.2) necessitate reinsertion of the tungsten vaporizer.

The dual vaporizer configuration offers the advantage that (non SP-) AMS data can be recorded when the laser vaporizer is turned off. However, turning the tungsten vaporizer off will not enable measurement in the single vaporizer SP-AMS configuration, as the tungsten vaporizer is also heated by the source of the 70 eV electrons. Recording (non SP-) AMS data is attractive since the (non SP-) AMS is well characterized, as it has been available for nearly a decade and is now widely used. For that reason, experimental campaigns in which fewer than two SP-AMSs are

available often employ the dual vaporizer configuration, as has been done in all the research presented in this thesis. Another advantage is that by comparing data acquired with and without the laser vaporizer, additional conclusions can be drawn regarding the particle constituents as detailed in sections 4.1.1.1 and 4.4.

3.1.2 Calibrations

The recommended practices for AMS calibrations can be found online[34].The two main procedures are briefly described below, with a short discussion of the property measured in each calibration.

3.1.2.1 Ionization efficiency calibration

The mass specific ionization efficiency[8] (*mIE*) is the sensitivity of the instrument to the plume produced by the vaporizer(s). In order to be part of the plume, the particles must first be vaporized. The (mass) fraction of the particles that is vaporized is referred to as the "collection efficiency" (*CE*) of the particles. *CE* is divided into three components[35] to explicitly treat losses due to: lens transmission (E_L), beam divergence (E_S) and bounce of the tungsten vaporizer (E_B), such that

$$CE = E_L * E_s * E_B \qquad [1]$$

The lens transmission (E_L) limits the size range of the instrument. Small particles are lost due to Brownian motion and large particles are lost due to impaction[36]. Particles in the range ~35 nm to 1.5 μm are focused by the lens[25], but E_L is reduced below 100 nm and above 600 nm (but near unity between 100 nm and 600 nm). Beam divergence (E_S) is dependent on particle morphology: aspherical particles have reduced E_S[35]. Since the laser vaporizer (soot particle module) is narrower than the tungsten vaporizer, it is more sensitive to E_S[8]. Willis et al.[37] recently estimated that the recommended rBC calibration particles (further discussed below) have E_S 0.6 ± 0.1. Particle bounce (E_B), which is dependent on particle phase, normally dominates the tungsten vaporizer collection efficiency[38]. Typical E_B values are 0.25 for solid particles, 0.5 for ambient particles, and 1 for liquid particles. For ambient particles a parametrization introduced by Middlebrook et al.[39] is routinely used to account for E_B.

mIE calibration is performed by nebulizing an ammonium nitrate solution, and drying and size selecting the resulting particles using a Differential Mobility Analyzer (DMA). Particles with a mobility diameter of 300 nm are used, which have near unity CE[5]. Since ammonium nitrate is used as the standard calibrant, the *mIE* of other species is normally expressed in terms of relative ionization efficiency (*RIE*) with respect to nitrate. mIE_{NO3} is measured by varying the number concentration of

particles, and comparing the recorded signal intensity (ions/s) with the mass sampling rate (pg/s). The latter is calculated from the single particle mass (m_p), the volumetric sampling flow rate (Q) and the particle number concentration (obtained using a condensation particle counter [CPC]). When the instrument is calibrated, the volumetric mass concentration C of species s can be calculated as:

$$C_s = \frac{\sum_i I_{s,i}}{RIE_s * mIE_{NO3} * Q} \qquad [2]$$

in which i denotes the ion types generated and I is the ion rate.

Ideally, the RIE of each sampled species should be determined experimentally. As a minimum, ammonium nitrate and Regal Black (Cabot) *mIE* calibrations are required. During the calibration, it is important to minimize, and account for, the amount of multiply charged particles. (These inflate the calculated *mIE* as the actual mass concentration is higher than the number concentration measured with the CPC implies.)

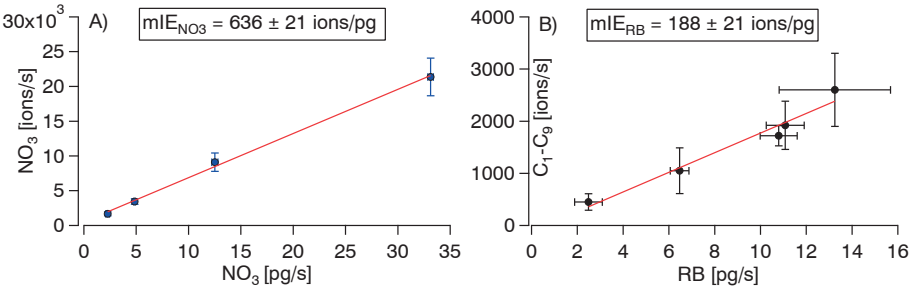

Figure 3. Mass specific ionization efficiencies of nitrate and Regal Black, obtained from nebulized 300 nm (mobility diameter) particles at an airbeam of 115 kHz, details in text. mIE uncertainties are 95% confidence intervals of the fitted slopes. The error bars show the variability (3σ) at each concentration.

Data from *mIE* calibrations with ammonium nitrate and Regal Black (RB, Carbot) are plotted in Figure 3. The *CE* has been folded into the *mIE* reported in Figure 3. While this is not expected to effect mIE_{NO3}, the true mIE_{RB} would be higher based on the results of Willis et al[37]. Although quantification in principle only requires the knowing the *product* of *CE* and *mIE* (i.e., the sensitivity of the instrument) ideally they should be separated, to give a better understanding of the processes involved.

The *mIE* values in Figure 3 are typical for the Lund University SP-AMS, but can vary considerably between deployments (and instruments). It is important to take note of the N_2^+ ion rate (the "air-beam" [AB]) during calibration. This value, 115 kHz during the calibration plotted in Figure 3 (also a typical value), is needed to produce quantitative results, as detailed in section 3.1.3. The AB is also needed to interpret the calibration result: high *mIE*/AB values indicate good instrument performance.

3.1.2.2 Size calibration

The sizes of aerosol particles are often expressed in terms of "equivalent diameters". Each equivalent diameter relates to a specified, measurable particle property. The particle's equivalent diameter is the physical diameter of a sphere of density 1 g/cm^3, which is equivalent, in terms of this property, to the particle. The two most commonly used equivalent diameters are mobility diameter (D_z) and aerodynamic diameter (D_a). These diameters and their relation are treated in detail by DeCarlo et al[40]. The AMS, because it is a vacuum system, measures the vacuum aerodynamic diameter (D_{va}). D_{va} is uniquely sensitive to the shape of the particles, which was exploited in Article V.

As the particles exit the aerodynamic lens, they acquire size-dependent velocities. The drag force from the accelerating gases is balanced by the inertial force acting on the particles such that smaller (i.e., lighter in relation to their drag) particles acquire higher velocities. The particle velocity (v_p) is commonly parameterized using the relation[41] below:

$$v_p = \frac{v_g - v_l}{1+\left(\frac{D_{va}}{D^*}\right)^b} + v_l \qquad [3]$$

in which v_g is the velocity of the gas exiting the lens, v_l is the velocity of the gas in the lens, D_{va} is the particle vacuum aerodynamic parameter (further discussed below), D^* is the characteristic particle diameter for acceleration in the expansion from the aerodynamic lens, and b is close to 0.5.

Calibration curves are obtained by nebulizing and drying polystyrene latex (PSL) spheres and fitting the expression [3] to the resulting data. As the PSL spheres are not promptly vaporized, the tungsten vaporizer is set to ~800 °C, and the leading edge of the PToF distribution is used to calculate v_p. (An offset of ~70 μs is added to the leading edge of the PToF distribution to account for the use of the first transmitted particles, rather than the average.) These should be verified with size selected ammonium nitrate particles, preferably including duplicates of the ones used in the ionization efficiency calibration (as the size of those particles is critical to that calibration).

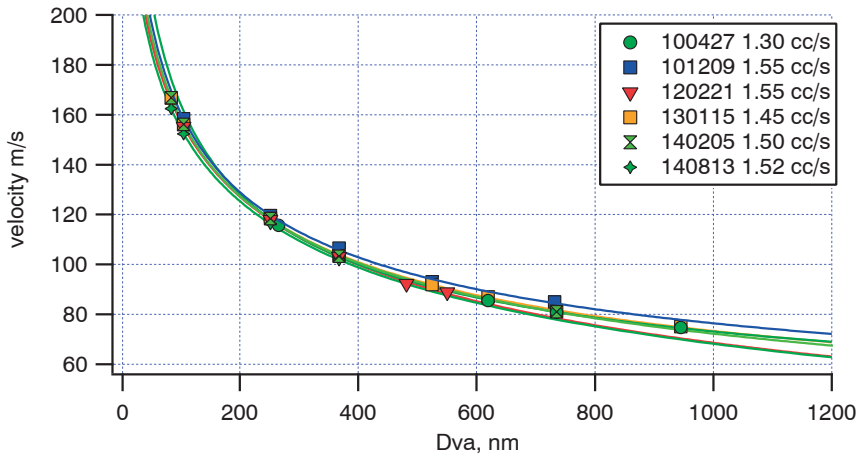

Figure 4. A sample of size calibration curves for the Lund University SP-AMS in the years 2010-2014.

Six calibration curves obtained for the Lund University instrument are plotted in Figure 4. Notably; the curve shapes are such that the calculated size of larger particles will be more sensitive to errors in the parameters used in sizing. The flowrate into the instrument (visible in the legend of Figure 4) is important to keep track of during measurements as reductions in flowrate (e.g., caused by clogging of the orifice) will often change the sizing by producing longer PToF. However, judging from the sample of curves in Figure 4, there is no general rule which relates flowrate and sizing (the effects of a reduction cannot be robustly predicted: a new calibration is needed for the data acquired at reduced flow).

3.1.3 Data analysis

SP-AMS data analysis is performed using the continuously evolving SQUIRREL and PIKA software programs which are available online[42].

As AMS data analysis is actually somewhat complicated, the following is a brief, bordering on simplistic, account.

The task of the analyst is assigning the ions formed in the plume(s) originating from the vaporizer(s) to chemical species. The ion rates, I in expression [2], need to be determined for each species. To this end, a "fragmentation table"[43] is employed. The fragmentation table lists the empirically determined fragmentation patterns of the species. While many of the default entries can be used, they do have to be verified, and to some extent modified, in each data set. For instance, the default entry of the organic component (OA) at m/z 44 is that all of the signal in this channel that is not attributed to air should be counted. This is because m/z 44 has a contribution from CO_2^+ ions that originate from carbon dioxide, one of the constituents of air. Thus,

the carbon dioxide contribution to m/z 44 needs to be calculated in order to quantify OA. For carbon dioxide, the fragmentation table entry at m/z 44 involves a reference to m/z 28, normally dominated by N_2^+ from molecular nitrogen, and the constant $370 \cdot 10^{-6}$, which is a leftover from the days when the ambient carbon dioxide mixing ratio was 370 ppmv. The analyst may have to introduce an additional factor (this makes the procedure more transparent than modifying the number $370 \cdot 10^{-6}$: it becomes easier to trace the steps) to account for increased CO_2^+ from nearby (or global) combustion. For the SP-AMS, m/z 44 has a third contribution: the CO_2^+ ions from rBC, further discussed in section 4.4.

Above, m/z 44 was used to introduce the fragmentation table. "m/z 44" actually refers to a mass-spectral region that is near the nominal 44 Th: by default ~43.8-44.2 Th. Thus, the example used "unit mass resolution" (UMR) data, in which the full m/z resolution of the instrument was not used. UMR analysis is performed with SQUIRREL. This type (UMR) should be used as a complement to the "high resolution" (HR) data. For size resolved analysis, only UMR data is normally used to reduce the complexity of the analysis, but there have been exceptions[44]. The results obtained from HR analysis can be compared with UMR results: they should be consistent.

High resolution analysis is performed with a model (PIKA) that explicitly accounts for the signals originating from a list of ions that the analyst chooses (uninformed choices will give spurious results). For instance, the signal at m/z 43 is normally divided into $C_2H_3O^+$ and $C_3H_7^+$, but several other ions exist which could potentially yield signals near m/z 43. PIKA parametrizes the peak width as a function of m/z, and postulates a constant peak shape. The residuals of the modeled and measured mass spectra are minimized by varying the ion abundances: the model does not decide which ions to include, or the time of flight (IToF) of each ion. The HR analysis employs a fragmentation table that is smaller than the table used in UMR as there are fewer instances where such apportionment is required (since there are more ion types than m/z's).

The signal from air is a very important aspect of the analysis. Despite the fact that (former) particle constituents are seven orders of magnitude more abundant (with respect to air) in the plume(s) compared with the ambient, air normally still dominates (which highlights how dilute the ambient aerosol is). It is recommended to insert a particle filter in the sampling line periodically. This way, the air signal can be studied in isolation, and guide the choices later made by the analyst. (I have found it is a good practice to filter the entire sampling flow, including what is sampled by other instruments, as a "zero-check".) The signal at m/z 28 is also routinely used to account for variability in sensitivity over time: using the "air-beam (AB) correction". The rationale is that many aspects of instrument performance will influence the AB and *mIE* in proportion. Care must be taken to ensure this assumed proportionality is real (by making several *mIE* calibrations). When sampling concentrated aerosol, it is also important to verify that particle signal is not misinterpreted as AB.

3.2 Auxiliary equipment

3.2.1 Smog chamber

Much of the literature on secondary organic aerosol (SOA) has been produced using smog chambers. The working principle of a smog chamber is that an aerosol is injected into a transparent chamber which is irradiated with UV light, and photochemistry occurs. Thus, atmospheric processing is simulated. We used a 6 m^3 fluorinated ethylene propylene (FEP) chamber (Welch Fluorocarbon), and UV lamps (Cleo Performance 100-R, Phillips) with peak emission at 350 nm (range 320-380 nm). The strength of the smog chamber set-up is that continuous processes, such as the gradual condensation of SOA onto soot particles (see sections 4.2.2 and 4.3) can be studied. Oxidant (chiefly hydroxyl radical) concentrations are typically elevated compared with ambient levels, but not by more than one order of magnitude. A caveat of smog chamber experiments is wall losses of particles and vapors[45, 46].

3.2.2 Potential Aerosol Mass chamber: PAM

The PAM chamber[47] is a small flow reactor that employs intense photochemical processing. The device is designed to robustly produce the maximum amount of secondary particulate mass in aerosols. To this end, the sample flow is subjected to oxidant concentrations that are two to three orders of magnitude higher than ambient levels, for short durations (minutes). A recent comparison[48] of PAM and a smog chamber found that ageing of wood smoke (and α-pinene, a biogenic SOA precursor) produced similar SOA in terms of amount and chemical composition. The PAM chamber has the advantage that particle losses are low (because of the short residence time). A caveat of PAM chamber experiments is that the intense processing favors new particle formation over condensation, even in when seed particles are present.

3.2.3 Aerosol Particle Mass Analyzer: APM

The APM[49, 50] (model 3600, Kanomax) consists of two concentric cylinders, in-between which an aerosol flow is drawn. By rotating the cylinders in unison (at an angular velocity ω) and applying a voltage (U) between them, particles are selected according to their mass (m_p) to charge (q_p) ratio, according to equation 4

$$\frac{m_p}{q_p} = \frac{U}{r^2\omega^2 ln\left(\frac{r_2}{r_1}\right)} \qquad [4]$$

in which r_1 is the radius of the inner cylinder, r_2 the radius of the outer cylinder and r is the average of r_1 and r_2. The instrument is operated by stepping the voltage and counting the selected particles with a condensation particle counter (CPC).

In the smog chamber experiments reported in Articles IV and V, the APM was used downstream a differential mobility analyzer (DMA) followed by thermal denuding at 300 °C for about 10 s (first DMA, then thermodenuder, then APM). Thus, we obtained mobility resolved particle mass with and without thermal denuding. The denuded mass was interpreted as BC, in qualitative agreement with rBC as measured with the SP-AMS, and with filter-based light absorption at 530 nm (measured with a particle soot absorption photometer (PSAP), which is similar to, but less sophisticated than the device described below in 3.2.4).

In Article V, the single particle masses (m_p) were extrapolated to the total particle ensemble using a scanning mobility particle sizer (SMPS). The SMPS provides the number concentration at each mobility diameter (D_z), and the DMA-APM provides the single particle mass (m_p) at each D_z. This facilitated the calculation of the (mass) mode fresh soot particle mass: 1.2 fg. Assuming a material density of 1.8 g/cm^3, the (mass) mode dynamic shape factor of the fresh soot was calculated as 2.2.

3.2.4 Dual-spot Aethalometer

The general principle of the Dual-spot Aethalometer[51] (model AE33, Magee Scientific) is that the aerosol is drawn through a filter where particles are deposited, while the light transmittance though the filter is measured continuously. Transmittance is recorded at seven wavelengths (λ) ranging from UV to near IR light: 370, 470, 520, 590, 660, 880 and 950 nm. In-situ attenuation by the particles is estimated from the change of transmittance though the filter over time. This is done assuming a constant (over λ and time) filter-material specific proportionality that takes into account the enhancement of the particle absorption resulting from scattering inside the filter matrix. In addition to the effect of in-filter scattering, filter loadings also impact the measurements. As the filter loading increases, the sensitivity is reduced: the filter begins to saturate. The filter loading effect is mitigated using dual filter spots with differing aerosol flow rate: the attenuation without loading effect is extrapolated from the two (differently loaded) filter spots[51]. The correction is applied at each λ separately. While attenuation (the sum of absorption and scattering) was measured, we estimate that the scattering was negligible in our experiments. We therefore use the term "absorption Ångström exponent" AAE, to describe the wavelength dependence of the measured attenuation. AAE is calculated as the negative slope of the log-log plot of attenuation versus λ, (i.e., if attenuation scales as λ^{-1}, the Ångström exponent is 1).

4. Results and discussion

4.1 Biomass combustion in residential facilities

We have conducted two measurement campaigns to elucidate particulate emissions from residential biomass combustion. The system most extensively investigated was a conventional wood stove (one of the most sold models in Sweden during the 1990s) further described by Pettersson et al[52]. The main finding of our first campaign was a marked difference in emission patterns between organic PM in general and particulate PAHs, which we reported in Article I. In the second campaign on which Article II is based, we added, among other things, photochemical processing and light absorption measurements to the set-up. This allowed us to investigate the emission of light absorbing carbon and prompted us to suggest a new metric to describe these emissions from energy-related activities: m^2/MJ.

4.1.1 Particulate PAH emissions

Particulate PAH emissions tend to escalate when the rate of combustion exceeds the appropriate range specific to the appliance used. In the wood stove we studied, nominally a 9 kW unit, a steep increase in emissions was observed above 23 kW (see Figure 3 in Article I). Such excessively intense combustion results in oxygen deficiency, which favors the emission of PAHs. This is unfortunate as some of them are known human carcinogens. The total organic PM emission rate by contrast is generally highest during the few minutes of heating and drying that follow the addition of a new batch of fuel: the fuel addition phase.

While the first campaign (Article I) had good reproducibility in the fuel addition phase emissions (100-200 mg of organic PM was consistently emitted upon fuel addition), the experiments in the second campaign (Article II) had much more variable emissions during fuel addition on glowing embers. In some cycles the characteristic “fuel addition peak” was absent or much above the average. The variable fuel addition emissions in the second campaign are in all likelihood more representative of real-world emissions. This is because the ignition of the volatiles produced upon fuel addition is a complex process that will differ substantially between cycles, even if the user behavior is almost the same. The high repeatability in

the first campaign, however, is more useful for attaining a mechanistic understanding of the governing processes.

The fuel addition phase emissions always contained some PAHs. Although the PAH fraction of the organic PM emitted was moderate (on the order of 1%) in many of the experiments that simulated optimal wood stove operation (the "nominal burn rate" cycles), the fuel addition emissions contributed the majority of the total PAH emissions. (The PAH content was low, but much organic PM was emitted). The PAH emissions during excessively intense combustion cycles ("high burn rate") were all dominated by the later "intermediate" phase. While avoiding fuel addition PAH emissions is near impossible, excessively high burn rates can be minimized. Factors that increase the burn rate include batch load, dryness and log size (using a lot of excessively dried wood in small pieces will produce unfavorably high burn rates).

The connection between combustion intensity, flue gas oxygen content, and PAH emissions is most succinctly illustrated by Figure 3 in Article I. The most informative data in that figure, denoted "high burn rate, intermediate phase with fuel addition" are further discussed below. The experiment consisted of two additional fuel additions in the middle of a combustion cycle, while the logs already in the stove were still ablaze. This is opposite to the default procedure of adding fuel only onto the embers of the previous batch of logs. The resulting flue gas oxygen concentration and particulate PAH emissions are shown in Figure 5.

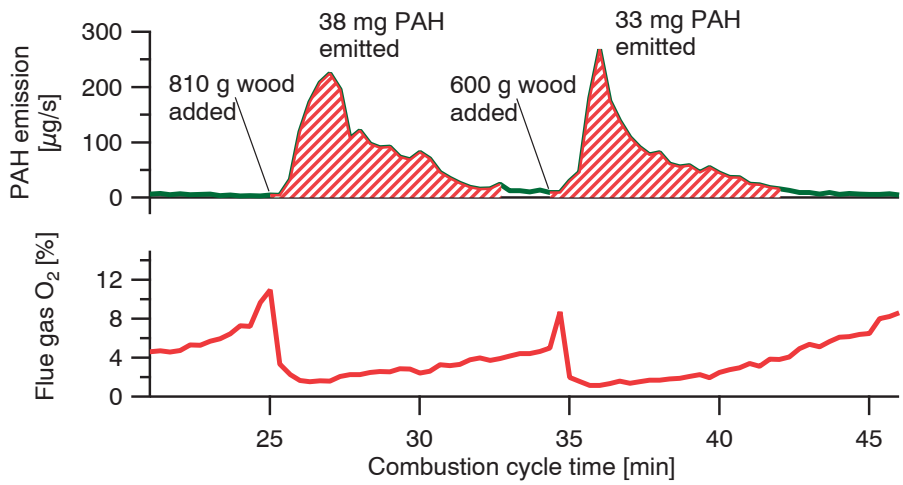

Figure 5. Particulate PAH emission and flue gas oxygen concentration during the "high burn rate, intermediate phase with fuel addition" experiment in Article I.

Around 24 minutes after the combustion cycle was initiated, and again ten minutes later, more fuel was added to the wood stove. The two additions each consisted of three logs, with a total dry weight of about 810 g and 600 g, respectively. Each fuel

addition was followed by a strong decrease in flue gas oxygen concentration as the rate of combustion increased, which resulted in elevated particulate PAH emissions. In the eight minutes following the first, slightly larger mid-cycle fuel addition, approximately 38 mg were emitted, and the second smaller fuel addition caused the emission of about 33 mg of particulate PAHs, again over a period of eight minutes. Not all of the pollutants formed originated from the two smaller batches added mid-cycle; some fraction was formed from the remnants of the earlier, larger batch that initiated the cycle. (Determining what fraction is very difficult with this set-up: it would require isotopically labeled wood! However, the point is entierly academic. What matters is that wood went in and PAH came out.) It is instructive to compare the ratio of mass of particulate PAHs emitted to fuel added: about 50 mg/kg, with full cycle values from Article I and refereces therein, 1.5 mg/kg for nominal burn rate, and 13 mg/kg for high burn rate cycles. The precision and accuracy of these values are discussed in the online supplement of Article I: the uncertainty is small compared with the differences in the comparisons made. It is then abundantly clear that user behavior will strongly influence real world emissions. There is nothing unusual about adding three pieces of wood weighing in total less than a kg about halfway through a wood stove combustion cycle.

4.1.1.1 High molecular weight PAHs

The first wood smoke campaign pre-dates our upgrade from AMS to SP-AMS (see section 3.1). For that reason, it was not possible to determine if the mass spectral patterns from large PAHs reported in Article I reflected the distribution of molecules in the wood smoke. Limited information is available in the literature regarding these molecules, as they are very difficult to measure using conventional analytical chemistry techniques. It was observed that the PAH distribution continued up to 48 carbon atoms (C48), with strongly decreasing abundances. However, it could not be exluded that this decrease was caused by the limitations of the (non-SP) AMS. Conceivably, the decrease could be caused by the instrument's inablitiy to efficiently vaporize the larger molecules. I have since aquired SP-AMS data during the second campaign, which will be used to answer this question here.

Figure 6 shows a comparison of data recorded with and without the soot module engaged. The experiment was performed by injecting PAH-rich wood smoke particles into a steel chamber and sampling them post injection. This was done in order to remove the variability of the stove output over time from the comparison. Comparing data with and without the soot module engaged, means a comparison between non-refractory (at 600 °C) particle content and anything in those particles likely to exist in significant amounts in aerosol particles, given that the latter broader class is internally mixed with species that absorb light at long wavelengths, such as BC (the main component of these particles).

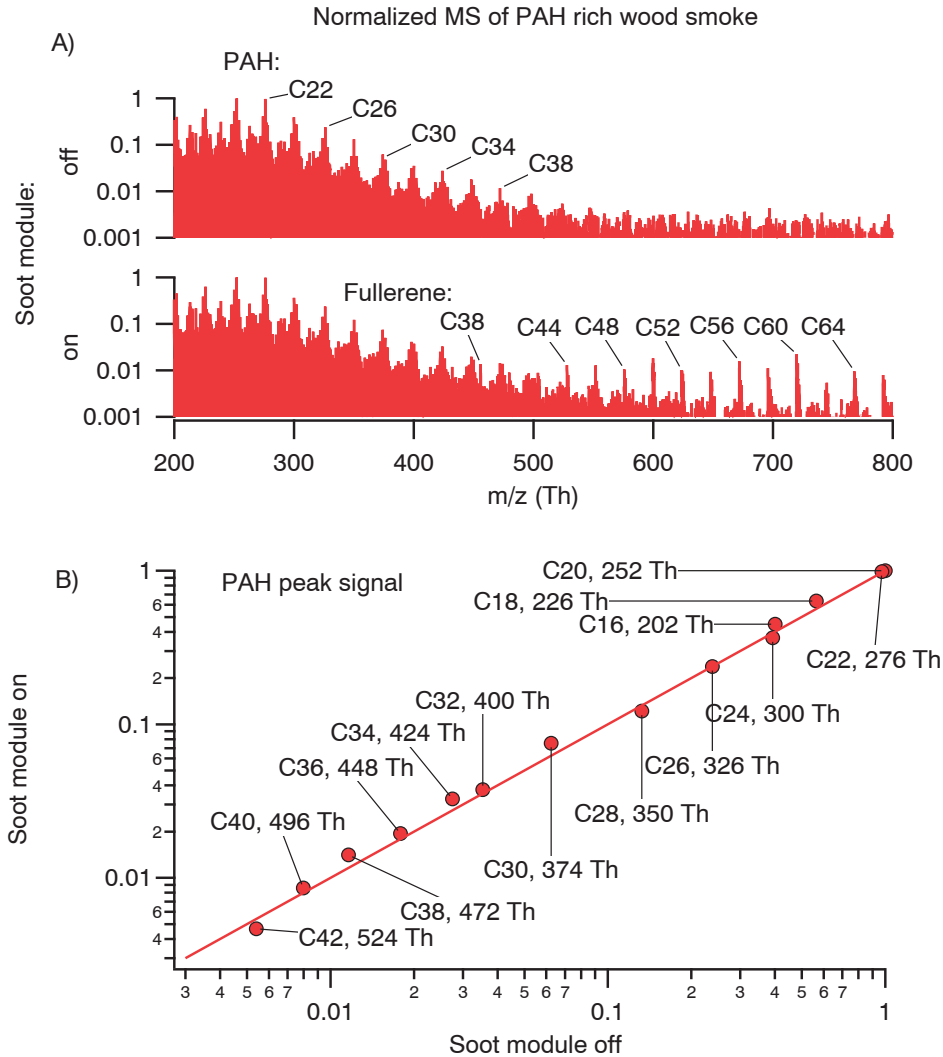

Figure 6. PAH-rich wood smoke measured with a dual-vaporizer Soot-Particle Aerosol Mass Spectrometer. A) Normalized mass spectra (m/z 200-800 Th) recorded with the soot module off (top) and on (bottom). B) scatter plot of normalized peak maximum intensities with and without the soot module engaged. Details in text.

The PAH signal intensity increased by about 60% when the soot module was engaged, which means a large fraction of the material was vaporized by the soot module. Hence, "non-refractory" was no longer a restraint imposed on the PAHs detected. The resulting mass spectra (the part of them that have a bearing on this discussion) are presented in Figure 6A above, normalized to facilitate comparison of the relative abundance of each peak. A scatter plot of the maximum intensities of 14 prominent peaks recorded with the soot module engaged versus disengaged is shown in Figure 6B. If the thermal stability of larger PAHs had a significant role in the

pattern observed by AMS, signals from large PAHs would be more enhanced than signals from small ones when the soot module was engaged. The data clearly show that the general pattern of decreasing abundance with PAH size is not an artifact of the AMS vaporization scheme. The data do reflect the actual distribution of the PAHs formed (some of the signal intensity decrease is due to the increasing fraction of multiply charged ions, but that is a minor effect).

This raises new questions. As the PAH abundance decreases strongly with carbon number (which is why signal intensity is plotted on a logarithmic axis in Figure 6 above, and Figure 4 in Article I), how large is the gap between large PAHs and small BC monomers? Are there any intermediates between the two that form in significant fractions from combustion? In other words, is the traditional dichotomy between elemental and organic carbon purely an arbitrary construct caused by limitations in instrumentation, or is there also an (admittedly, possibly loosely connected) underlying non-instrument specific split? The fullerenes shown in Figure 6A may not count, as it is possible they were mainly formed in the instrument, and not in the combustion process. Fullerenes are known to form from BC heated by high intensity lasers such as the one used in the soot module.

In recent investigations of PAH rich soot, we extended the measured m/z range up to about 4 kTh without finding any additional PAH signals, which implies that few PAHs in the C50-C300 range are emitted. Given that a very, very small (5 nm in diameter) BC monomer contains roughly 6000 carbon atoms, the split seems justified barring emissions of significant amounts of fullerenes formed in-flame. In fact, even in the hypothetical case with significant fullerene emission from flames, it could be argued that the split is justified, as these (fullerene) carbon atoms belong on the "elemental" side of the carbon split due to their lack of bonds with non-carbon atoms, and thermal stability.

4.1.2 The color of wood smoke

Biomass burning is a known source of brown carbon (BrC), carbonaceous PM which absorbs light with a strongly wavelength dependent efficiency[53, 54]. BrC is conventionally considered a subcategory of organic carbon. A recent study[55] showed that BrC emission depends on the combustion conditions rather than fuel species. The authors also reported that BrC absorption increases, and the wavelength dependence of the BrC absorption decreases with increasing BC to OA ratio. In addition to primary sources, BrC is also known to be formed from secondary processes, including photochemically induced gas-to-particle partitioning[54] (i.e., some BrC is SOA). Specifically, BrC has been observed in SOA formed from aromatic precursors[56], such as benzene, which is emitted from wood stoves (and other sources). UV light has also been demonstrated to bleach BrC[57], which makes the coupling somewhat complicated. BrC is of interest due to its direct climate heating effects, and

as an inhibiter of atmospheric photochemistry, by reduction of UV light[58], which drives the reactions. Furthermore, the wavelength dependence of PM absorption is commonly utilized for source attribution; as traffic (chiefly diesel engine) emissions are known to exhibit weak wavelength dependence, enhanced dependence is attributed to biomass burning.

The experiments reported in Article II feature wood stove emissions that were measured with a Dual-spot Aethalometer (see section 3.2.4). The calculated absorption Ångström exponents (AAE, a measure of the wavelength dependence, see section 3.2.4) for full combustion cycles were surprisingly low –around 1.1 for nominal burn rate (intended stove operation) and 1.2 for high burn rate (excessively intense combustion). High AAEs such as the ones assumed in source attribution efforts[59] (~2) were found only during the fuel addition phase, when the combustion was colder and less intense. The fuel addition emissions generally contribute a small fraction (<10%) of the full cycle light absorbing carbon emissions. Consequently, the wood smoke produced in our study, using a conventional, reasonably well-operated stove, would be misattributed as traffic emissions using the "Aethalometer model[59]" approach, which assumes high AAEs for wood smoke.

Due to the possible coupling between BrC and UV light outlined above, photochemical processing was performed on the wood smoke using a Potential Aerosol Mass chamber (se section 3.2.2). Interestingly, the processing generally had little impact on the measured light abdorbing carbon concentrations (LAC, see "Soot and related terms"), in spite of substantial SOA formation in the high burn rate experiments. Two photochemical ageing experiments were performed on the fuel addition smoke, which in contrast to the full cycle emissions had significant BrC content (i.e., the AAE was ~2.5 rather than ~1). In the two experiments, BrC reductions of ~30% and ~10%, respectively, were observed under intense photochemical processing. This indicates the BrC produced in our experiments was fairly insensitive to both UV-induced bleaching, and oxidation by OH or O_3.

High BrC emissions in the early stages of the combustion cycle were previously reported for bituminous coal combustion[60]. This phase, termed the "fuel addition phase" in our studies, was identified as in Article I as exhibiting high OA emission rates (as discussed above in section 4.1.1). Figure 7 shows time resolved AAE (top panel), rBC, 950 nm light absorbing carbon (LAC 950) and OA concentrations measured during a nominal burn rate cycle. Notably, the AAE is higher in the fuel addition phase than during the rest of the cycle.

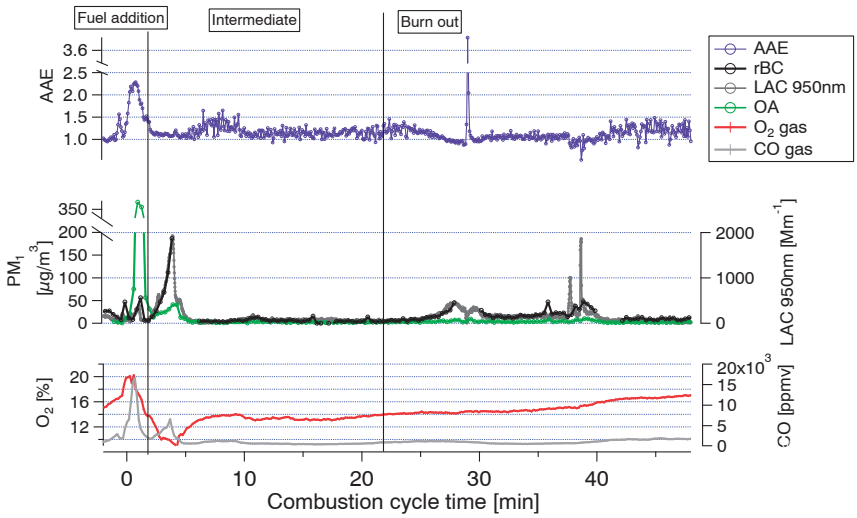

Figure 7. Absorption Ångström exponent (top), diluted flue gas PM concentrations (middle), and oxygen and carbon monoxide concentration (bottom) during a nominal burn rate cycle. Gaps in rBC data are due to disengaged soot module (see section 3.1.1). Figure 1 in Article II.

Several lessons can be learned from studying Figure 7, both about the processes studied and the methods employed to study them. Firstly, the highest rBC (and LAC 950) emission rates occurred during the most intense combustion, around 2-5 minutes into the cycle when the flue gas oxygen content was around 10% (which is still moderately intense combustion compared, for example, with Figure 5 above.) Although this part of the cycle had the highest BC emissions, elevated BC emissions were also measured at cycle times 26-30 minutes, and 38-40 minutes. These emissions did not coincide with an overall high combustion intensity, as the flue gas oxygen content was high, around 15%. This implies local conditions in the combustion chamber that have little impact on the average flue gas composition can influence BC emissions considerably.

A closer inspection of the two later episodes (t=26-30 min, 38-40 min) reveals that the default SP-AMS operation (see section 3.1) employed in these experiments did not capture the full dynamic of the emissions. Some rapid transients were not captured, owing to the limited time resolution (10 s) and the large fraction of time spent quantifying the instrumental background. The general features were captured, such as the high OA emissions after fuel addition and the elevated BC and particulate PAH emissions at high burn rates. Llimitations in time resolution can be avoided in future experiments by using the "fast-MS[61]" mode of operation, which enables 1 Hz sampling (thus matching the Aethalometer time resolution). Fast MS also considerably improves the duty cycle. (The two brief LAC 950 emission spikes at t~38 and 39 minutes are most likely underestimated in the SP-AMS due to overlap with "closed" sampling [see section 3.1] where instrumental background, and not PM

mass concentration, is quantified.) Fast MS can be used with little extra cost in terms of work load for the analyst (considerably more disc space and computing time would need to be allocated, but these are not the limiting resources!).

Finally, the highest AAE observed, which occurred around t=28 min (see Figure 7), while too brief, and coinciding with too low LAC concentrations to be of any significance for the total LAC emitted in this cycle, may still be very informative. Note that AAE is a measure of the quality of the LAC, not the quantity, and as such, distinctly different from the rest of the data in Figure 7. The measured LAC concentrations across in AAE peak were roughly constant at UV wavelengths, altogether gone at IR wavelengths, and correspondingly reduced in the visible range (such that the longer wavelengths were more reduced). However, without supporting data this finding is difficult to interpret, and may even conceivably be an artifact. This is a general feature in experimental aerosol science: conclusions based on data from only one instrument, regardless of which instrument, are often tenuous. The work reported in Article IV for instance, while mainly based on AMS data, would not be possible without the co-sampling Scanning Mobility Particle Sizer (SMPS). The same is true for Article V and the APM (see section 3.2.3).

To adequately describe emissions, they must be related to the extent of the activity which generates them. In Article I for instance, the central measure of particulate PAH emissions is mg/MJ. This is because the comparison between the different modes of operation – nominal and high burn rate – would be misleading unless the difference in heat output was taken into account. To ease cross referencing the alternative mg/kg dry fuel is also used in the article. In Article I, the quantity mg/MJ was calculated by multiplying the mass concentration by the volumetric flow rate in the chimney and time elapsed (which gives the mass emitted) and dividing the product by the heat generated, which was calculated based on the oxygen consumption method[62]. As the quantity measured by the Aethalometer is attenuation (see section 3.2.4), which has the unit m^{-1}, rather than mass concentration, the analogous calculation in Article II yields m^2/MJ (at each wavelength) as metric for light absorbing carbon emissions. Using this metric, we found higher (on the order of +50%) light absorbing carbon emissions from high burn rate cycles compared to nominal ones.

While the basis for introducing m^2/MJ to quantify light absorbing carbon emission was to eliminate the dependence of our results on assumed mass attenuation coefficients (which are routinely used in the literature to estimate mass concentration from attenuation measurements), there are others benefits as well. When the light absorption itself is the quantity of interest, optically defined emissions are more relevant. For instance, when assessing the PM direct effects in radiative forcing, or the impacts on UV photolysis rates.

4.2 Smog chamber ageing of light duty vehicle emissions

Light-duty vehicles are a significant source of PM. Since there is considerable uncertainty in how the exhaust transforms after emissions, we performed smog chamber experiments that simulated atmospheric ageing processes (see section 3.2.1). For gasoline exhaust, we investigated the extent and origin of secondary organic aerosol (SOA) formation. Diesel car exhaust ageing was also investigated, specifically how the soot particles interact with water and how their shapes develop after emission.

4.2.1 Gasoline exhaust

Gasoline-fueled vehicles generally emit little primary particulate matter[16]. They do however emit significant amounts of precursor gases, such as nitrogen oxide, ammonia, and volatile organic compounds, from which secondary PM eventually forms. While exhausts from gasoline vehicles do not contribute much to ambient BC loadings[13], gasoline exhusts are generally co-emitted with diesel soot, and consequently play a role in soot transformation.

In Article III, we reported secondary organic PM (SOA) formed in photochemically aged exhausts from idling light-duty vehicles during smog chamber experiments. One to three orders of magnitude more secondary PM was formed than what was emitted directly in our experiments. Furthermore, we contrasted the gasoline exhaust SOA with SOA formed from pure precursor mixtures, by comparing the mass spectral signatures and mass of SOA formed per precursor mass reacted ("SOA yield"). Based on this comparison, we conjectured that additional precursors present in the exhaust (other than the C6 to C9 aromatic compounds in the exhausts thought to contribute to SOA formation) accounted for more than 40% of the SOA formed. In spite of this, the SOA formed from a few, pure precursors was surprisingly similar to the SOA formed in the engine exhaust. Their elemental composition (H:C 1.4±0.2, O:C 0.4±0.1), and volatilities (inferred from thermal denuding, discussed below) were about the same.

While the main focus of Article III was the carbonaceous secondary PM formed, significant fractions (30-70%) of the secondary mass formed in the exhausts were due to nitrates. Some of the nitrate was chemically bonded with the carbonaceous fraction, corresponding to 3-8% of the latter by weight, but the majority occurred in the form of ammonium nitrate (the two can be distinguished because the ratio NO^+ to NO_2^+ ions is higher for ammonium nitrate, and by the abundance of ammonium). Figure 8 shows the wall-loss corrected time series recorded in experiment I1 in Article III. The nitrate has been divided into organic (bound to carbonaceous fraction) and inorganic nitrate, assuming NO^+/ NO_2^+ ratios of 0.2 (the lowest observed ratio, which

occurred in experiments without secondary particulate ammonium) and 0.65 (measured for ammonium nitrate during the campaign), using the parametrization introduced by Farmer et al[63] .

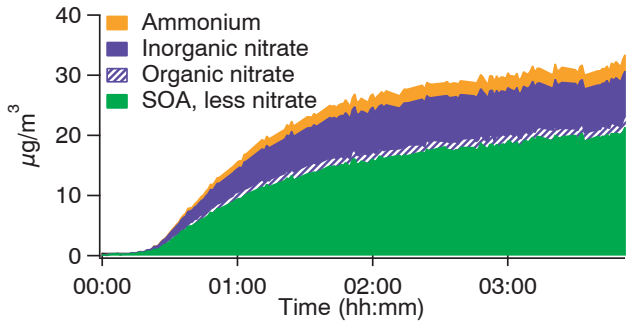

Figure 8. Wall loss corrected timeseries of secondary PM formed in experiment I1 in Article III. Time=00:00 indicates the start of UV irradiation.

Thermograms were obtained in selected experiments by heating the sampling flow to temperatures up to 100 °C during approximately 6 s, and removing vapors using activated charcoal. (The thermodenuder used was previously described by Jonsson et al[64].) As the ammonium sulphate seeds used in the experiments do not volatilize at such temperatures, and the particle number concentrations recorded imply internal mixtures, the sulfate signal was used to remove the combined effects of thermophoresis, smog chamber wall losses, and instrument collection efficiency (see section 3.1.2.1) from the data.

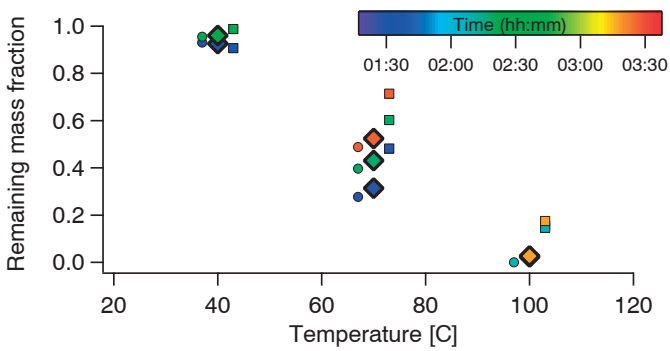

Figure 9. Nitrate thermograms recorded in experiment I1 in Article III. Total (diamonds), inorganic (circles, negative temperature offset) and organic (squares, positive temperature offset) nitrate, colored by time from UV onset.

Figure 9 shows the nitrate thermograms of experiment I1 (in Article III), where the deconvolution of nitrate outlined above (as in Figure 8) has been applied. The ammonium nitrate in these particles was significantly less prone to evaporate upon heating than pure ammonium nitrate particles, which were previously studied using the same thermodenuder[65]. The same observation – retarded ammonium nitrate losses from thermal denuding (compared with pure ammonium nitrate particles) – has been made in urban air[66]. It is likely that the low loss of ammonium nitrate upon heating is a consequence of kinetic limitations imposed by the increasing amount of SOA present in the particles. This would explain the increase of remaining mass fraction with time. This hypothesis carries the implication that in such experiments, where brief (a few seconds) heating is used to classify PM volatility, the phase and mixing state comes into play as well as intrinsic, molecular properties such as saturation vapor pressure and enthalpy of vaporization. The same would be true for isothermal dilution of the aerosol, unless sufficient time was allowed to pass between dilution and measurement, and equilibrium conditions were achieved. Thus, inferences made about the chemical composition of aerosol particles based heating or diluting the aerosol briefly would be confounded.

Nitrate groups were fairly abundant in the SOA formed in experiment I1. Assuming an average (by mass) SOA molecular weight of 200 Da, the ratio of nitrate groups to SOA molecules was approximately 1:4. Upon heating to 100 °C, this ratio decreased to about 1:10. This could be because the organic nitrates were more volatile than the average SOA. However, thermal decomposition of the SOA molecules could also explain this observation.

4.2.2 Diesel exhaust

Soot particles from a diesel-powered light-duty vehicle were investigated as potential cloud condensation nuclei (CCN) in Article IV. Fresh emissions were injected into a smog chamber (see section 3.2.1), and photochemically aged together with light aromatic SOA precursors. In this manner we studied the entire range of diesel soot transformation, from freshly emitted black carbon particles lightly coated with hydrophobic primary organic PM, to particles dominated by (somewhat) hygroscopic secondary organic PM, grown with the fresh particles as seeds.

Some CCN activity was observed immediately (defined by the time resolution of the measurement, that is, in less than five minutes) after the onset of UV light. As the photochemical ageing proceeded, the particles became progressively more efficient CCN. With the exception of the very early stages of the transformation, the particles' ability to activate into cloud droplets could be accurately modelled assuming constant (independently derived) SOA properties using κ-Köhler theory[67, 68]. Key inputs to the modelling exercise were the mobility-resolved particle mass, and its volatile fraction as measured by the APM (see section 3.2.3). Furthermore, particle shapes were

implicitly taken into account by using the volume equivalent particle diameters (see section 3.1.2.2). During the initial stages however, the measured CCN activity was consistently lower than what was modelled. As the condensed mass fraction increased, the modelled and measured CCN activity converged; above roughly 10% condensed mass, they were in agreement.

One possible explanation for the rapid UV-induced CCN activity is the heterogeneous conversion of NO_2 into nitrous acid on the soot surfaces, a process which is known to occur[69] and has been demonstrated to be enhanced drastically under UV irradiation[70]. Water soluble material could thus conceivably be added to the diesel soot over short timescales; nitrogen containing species could be involved in the initial water uptake. Although the time traces look somewhat different, each experiment featured an increased average carbon oxidation state (OS_C) and nitrate formation on the onset of UV light. In experiment DEP2 in Article IV, a rapid increase in OS_C and NO^+ ion intensity occurred within a few minutes after UV lights were turned on (Figure 10). The increase of NO^+ ions corresponded to roughly 1‰ of the PM mass. The OA exhibited increased OS_C throughout the ageing. The overall time dependence, a gradual increase (see Figure 2, Article IV) of OS_C was likely caused by condensation of more oxidized SOA on reduced POA (for instance, lubrication oils). The more sudden OS_C increase in Figure 10 around t=4 minutes, by contrast, seems to be the result of a rapid chemical transformation of the condensed phase (as there is no corresponding increase in OA mass to explain the OS_C shift from -1.4 to -1.1)

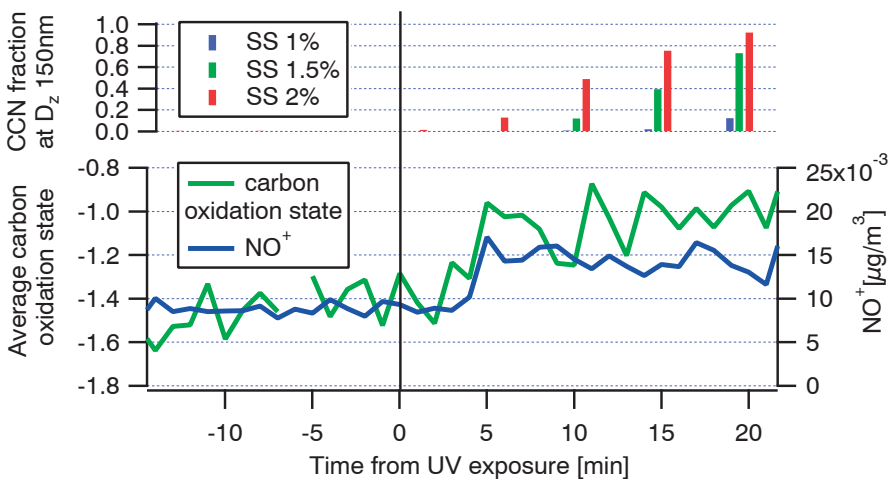

Figure 10. Cloud activation at mobility diameter 150 nm (top) and polydisperse average carbon oxidation state (bottom) and NO^+ signal in experiment (bottom) DEP2 of article IV.

The κ-Köhler modelling reported in Article IV, which assumes constant SOA properties, overestimates the initial CCN activity. Either the discrepancy is caused by an intrinsically different SOA or there is some extrinsic, CCN activity repressing effect in play which is more pronounced in the early stages of the ageing. While the data does not unambiguously exclude either explanation, it is not unlikely that the cause of the low CCN activity is intrinsic to the SOA. It is conceivable that the initial low concentration of OA favors the condensation of larger SOA molecules, which have lower saturation concentrations. Larger SOA molecules would, all other things being equal, explain the discrepancy between modelling and measurement in the early stages of the ageing. However, the main finding is the close agreement between modelled and measured CCN activity for diesel soot for the majority of the ageing process.

Besides enabling water uptake, the secondary organic aerosol condensation was found to induce morphological changes in the diesel soot. Consistent with recent findings by Schnitlzer et al.,[71] who worked with diesel soot proxies (burner soot) and SOA from aromatic precursors, the reshaping process was rather slow in our experiments. At first, the shape changed due to the filling of open structures in the soot agglomerate. In the later stages, when most of the particle mass was secondary, the soot cores began to restructure. This restructuring was irreversible; when the coatings were removed, the shape was still different from that of the freshly emitted soot.

In our experiments, diesel soot ageing though SOA condensation was studied under dry conditions. One of the parameters investigated (but not reported in Article IV) was particle water uptake in sub-saturated (RH 90) air: the hygroscopic growth factor (HGF). HGF was measured in terms of mobility diameter (D_z), which is the conventional approach. Contrary to D_{va}, asphericity in particles translates into *larger* D_z. The experiments consistently featured HGFs below unity, which indicates that restructuring of the particles occurred due to water uptake. This restructuring was observed to begin early in the ageing process, where most of the particle mass (>80%) was still BC. Thus, liquid water condensation was found to accelerate the diesel soot restructuring.

4.3 Ambient measurements

In ambient air, chemical species have characteristic distributions over size in PM_1. Particulate nitrates, sulphates and ammonium are predominantly found in the accumulation mode, which in terms of mass often peaks in the 500-800 nm D_{va} range (see 3.1.2.2). Organic aerosol (OA) is also found in the accumulation mode, but typically with a "tail" towards smaller diameters, indicative of recent (hours to one or a few days) condensation. Sometimes, but not always, this follows new particle formation. However, OA which has condensed on accumulation mode particles will

also contribute to the "tail". In and downwind urban centers, the "tail" is overlaid with fresh traffic emissions, which mostly consist of black carbon (BC) and OA (see Figure 11). This OA has mass spectral features which are consistent with lubrication oil. BC is unique among the major PM_1 constituents, in the sense that it is exclusively primary and non-volatile. Freshly emitted BC is also uniquely aspherical, while aged BC-containing particles are close to spherical, like most non BC-containing particles. Consequently, the distribution of BC across PM_1 and the evolution of this distribution with atmospheric ageing, are very informative.

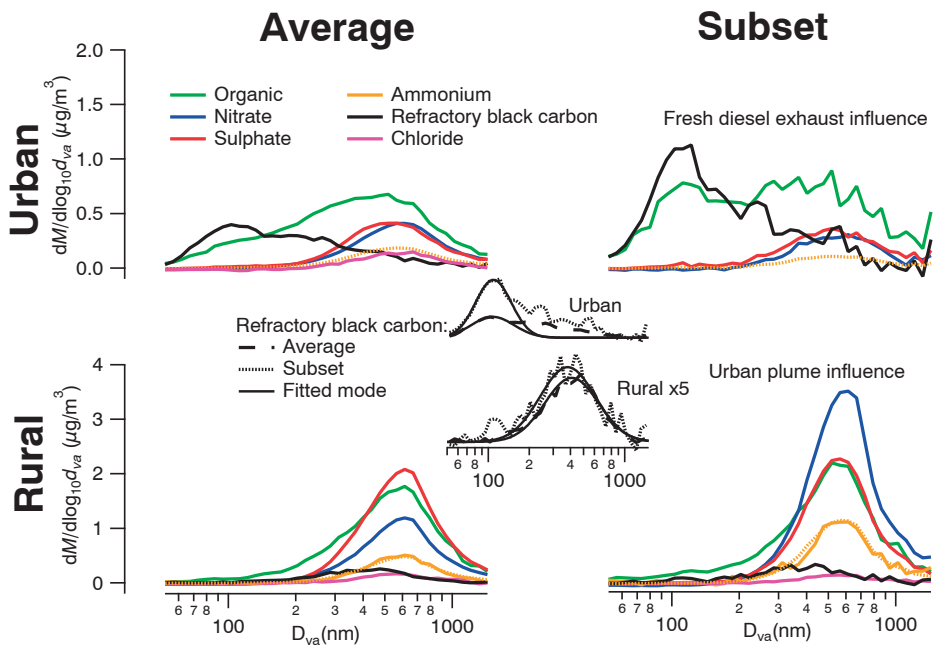

Figure 11. Ambient, chemically resolved D_{va} distributions. Top: urban air, bottom:rural air. Left: campaign averages, right: subsets with enhanced influence from fresh diesel exhaust (top) and urban plumes (bottom). Center: refractory black carbon distributions in isolation. Figure 1 in Article V.

Article V is based on D_{va} resolved SP-AMS data from smog chamber experiments (see section 4.2.1) simulating diesel exhaust ageing, combined with ambient observations made in urban and rural air. The urban sampling was conducted at a curbside site in Copenhagen[72], and the rural data was recorded at the ACTRIS[73] regional background site Vavihill[74], situated approximately 60 km from downtown Copenhagen. Both campaigns were carried out in wintertime, in consecutive years.

The average urban PM_1 distribution was dominated by accumulation mode particles (Figure 11). The proportion of local and transported PM_1 in urban air depends on many factors, (both meteorological and related anthropogenic activities), but similar

observations have been made for other cities. A recent study[75] found that even in the considerably larger city of Paris, regional contributions dominate.

A subset of the urban data was defined based on the ratio of rBC to OA. As the purpose of the study (Article V) was to elucidate diesel soot transformation, the subset was designed to enhance the influence on the urban data from fresh diesel exhaust. For this purpose, all periods (dt=1 min) with more rBC than OA were selected. The rationale behind the design was that fresh diesel exhaust particles are dominated by rBC (in contrast to to all other major sources).

In the rural data, another subset was defined based on air mass back-trajectories. The purpose of the rural subset was to enhance the influence of the urban plumes. All back trajectories that had passed over Copenhagen (dt=1 h) were included. This was done on the entire dataset, and the conclusions drawn from comparing average and subset (further discussed below) were further verified by two complementary analyses. First, the exercise was repeated on air masses of south-western origin only (the general direction of the city from the regional background site), to remove the possibility of confounding the results due to differing source regions. Second, back trajectories of northern origin were selected to further enhance the relative contribution of the city, at the expense of the extent of the comparison (the number of hours included) and signal to noise ratio.

Atmospheric transformation was found to have moved the freshly emitted diesel soot well into the accumulation mode (Figure 11, center). As the average (over rBC abundance) modelled transport duration was a mere five hours, this was an unexpected finding. While suggested transformation timescales in the literature vary from hours to weeks[76], this is to my knowledge the first report of rapid transformation despite such limited photochemistry. A cumulative hydroxyl radical exposure of $0.4 \cdot 10^6$ molecules/cm^3 · h was modelled using the process model ADCHEM[77]. Given that photochemistry is considered to be the main driver of atmospheric transformation of PM_1, one would expect rather small changes to occur during the first five hours of plume evolution under these conditions.

The smog chamber data show that in order to move fresh diesel soot into the accumulation mode, substantial amounts of SOA (around ten times the original particle mass) are required under dry conditions (Figure 12). D_{va} is determined by shape and mass (see 3.1.2.2). The mass (1.2 fg) and mass weighted dynamic shape factor (DSF, 2.2) of the fresh diesel soot studied in the laboratory was calculated from Aerosol Particle Mass analyzer and Scanning Mobility Particle Sizer data (see section 3.2.3). Using this mass and shape, the ambient data were reproduced with reasonable accuracy (Figure 12). In order to approach the accumulation mode however, particle shape must change. The reason such extensive SOA coating was required is that this effect (decreased DSF due to agglomerate restructuring) occurred late in the experiments, consistent with recent studies of artificial burner soot[71].

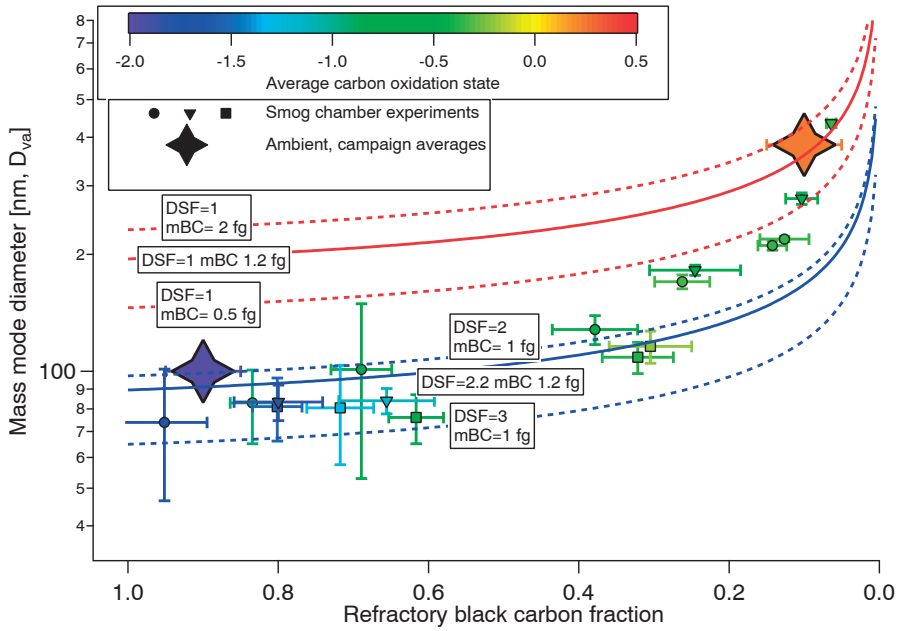

Figure 12. Diesel soot transformation in the smog chamber and ambient air: D_{va} versus rBC fraction. Three smogchamber experiments with diesel soot (small circles, triangles and squares) and ambient campaign averages (large stars). Effects of BC mass and shape (dynamic shape fractor, DSF) illustrated by lines. Details in text. Figure 3 in Article V.

While much SOA is required to complete the soot restructuring, there are other, more efficient potential reshaping agents available in ambient air. Sulphuric acid for instance, has been demonstrated to efficiently reshape diesel soot proxies[78, 79]. In all likelihood soot restructuring is linked to the surface tension of the condensing species; higher surface tensions are expected to restructure particles more efficiently. As water also has high surface tension, and is present in great abundances, more so than other vapors by orders of magnitude, it is a very likely candidate to have caused the rapid ambient soot transformation observed in Article V.

In order for liquid water to have caused the reshaping observed, the diesel soot in the urban plumes must have rapidly acquired hygroscopic coatings. The air mass back-trajectory guided mass spectral analysis strongly suggests that this role was mainly played by ammonium nitrate. While SOA was found to enable water-induced restructuring (see section 4.2.2), ammonium nitrate is expected to be much more efficient, as it contains a higher density of soluble entities (by an order of magnitude, assuming an SOA molecular mass of 200 Da and one water soluble entity per SOA molecule).

4.4. Black carbon heteroatoms

Black carbon (BC) is formed during high temperature incomplete combustion of carbonaceous fuels. The process, outlined in Figure 13, involves loss of hydrogen from the unburnt fuel as it is graphitized. The completeness of the graphitization process, and hence fraction of hydrogen lost, varies depending on the source. This is because the characteristic combustion processes of the sources differ. Different fuel mixtures are combusted, and at different temperatures and pressures. BC is highly stable under ambient conditions (hence, there is prehistoric artwork drawn with soot which still remains). In the combustion process however, BC is to a large extent an intermediary. In diesel engines for example, it is well known that most of the BC is *completely* oxidized in the cylinder (and hence, not emitted). As the processes involved are inherently variable, it would be unexpected if the oxidation process was "all or naught". Partial oxidation of some (if not all) BC monomers seems more likely: one could expect oxygen containing functional groups in the outer layers. In fact, it would be puzzling if there were no heteroatoms (i.e., non-carbon atoms) present in the BC since the original materials (diesel fuel, wood, etc.) all contain substantial amounts of hydrogen, and the flames from which the particles originate are highly oxidizing environments.

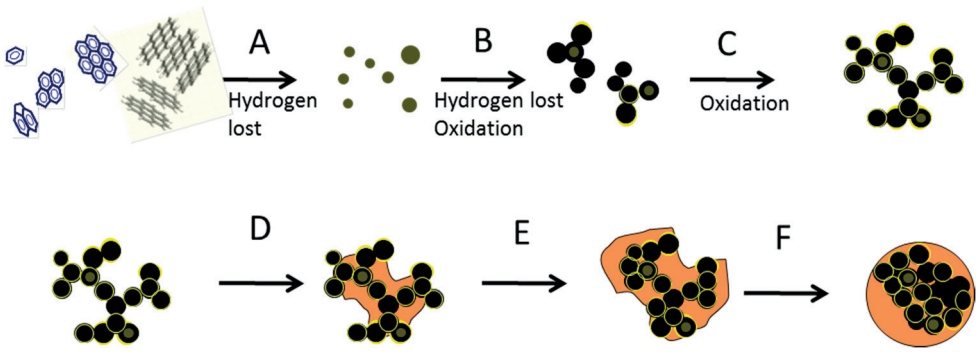

Figure 13. Conceptual illustration of soot formation and transformation, with suggested origin of BC heteroatoms: hygrogen (brown) and oxygen (yellow). **A**) BC monomers are formed through PAH growth. **B**) Monomers graphitizise, oxidize and coagulate into agglomerates. **C**) Agglomerates undergo further oxidation (often complete oxidation, stopping D-F from occuring). **D**) Agglomerates are coated by condensing material upon reduction of temperature after emission. **E-F**) Further atmospheric condensation of secondary PM which induces algglomerate restructuring. A-C: in flame, D-E: fresh plume, F: aged plume.

Refractory oxygen-containing material was consistently found in the SP-AMS studies reported here (Articles II, IV, V), which could be unambiguously assigned to rBC (i.e., oxygen that was not part of the organic aerosol). The details of this deduction are discussed below. Oxygen- and carbon-containing ions originating from rBC

($rC_xO_y^+$) were identified in diesel exhaust, wood smoke, and ambient air heavily influenced by fresh traffic emissions. The $rC_xO_y^+$ ion abundances seem to always follow the following rule: $rCO^+ > rCO_2^+ > rC_3O_2^+$ (this empirical rule holds beyond the work presented here). However, as rCO^+ is masked by the neighboring N_2^+ peak (typically corresponding to ~100 nitrate equivalent μg/m^3), it is normally below detection limits in ambient-relevant PM_1 concentrations, despite high ion abundance. This issue can be overcome by reducing the molecular nitrogen content of the aerosol (the normal fraction is 0.8), by sampling the particles in an argon atmosphere (the alternative is sampling more concentrated PM_1) as was done for wood smoke in Figure 14.

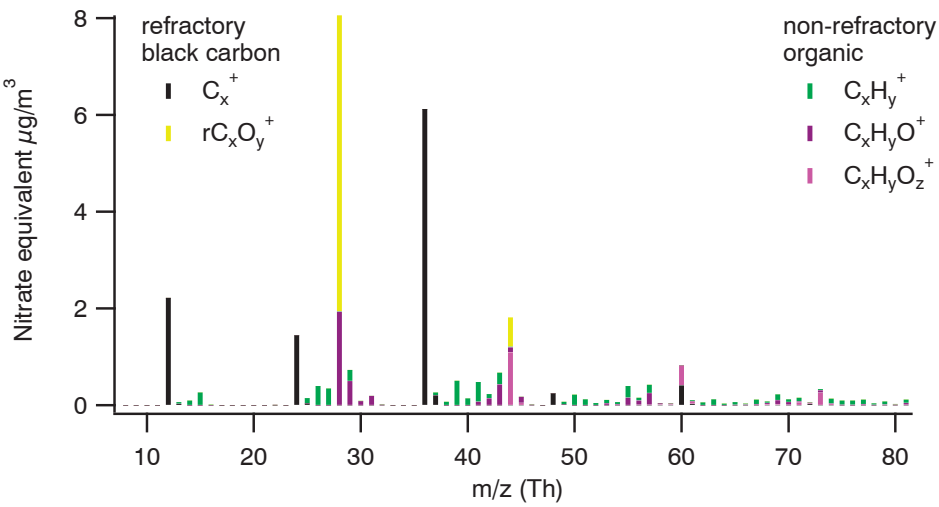

Figure 14. Wood smoke from the stove studied in Article I-II, emitted in the intermediate phase of a nominal burn rate cycle (representative of emissions from appropriate stove operation). The aerosol was diluted with argon, to reduce mass spectral interferences.

Notable peaks in the wood smoke mass spectrum (Figure 14) include pure carbon clusters, CO^+, CO_2^+, and the fragments originating from mono-saccharides such as levoglucosan at 60 and 73 Th. The mono-saccharide peaks, which originate from organic coating and not rBC, are often used for source attribution of wood smoke in ambient air[80]. While the pure carbon peaks are entirely dominated by rBC contributions, CO^+ and CO_2^+ can have significant contributions from non-refractory PM as well. The assigments of CO^+ and CO_2^+ to rBC were done using the "fragmentation table" approach (see section 3.1.3). The C_3^+ signal was used to calculate rBC fractions (in these experiements the ratios of rCO^+ and rCO_2^+ to C_3^+ were found to be 1±0.1 and 0.1±0.03, respectively). In the example spectrum in Figure 14, the non-refractory organic contribution to CO^+ is rather small. This is consistent with the fact that the other organic peaks make up a limited fraction of the full MS.

In order to make the split between the rBC and OA signal, the flexibility of the dual vaporizer (see section 3.1.1) configuration can be used. From scatter plots of data recorded with and without the laser vaporizer (soot module) engaged, conclusions can often be drawn as to which ions have significant rBC contributions (thus identifying signals from BC heteroatoms). Both rBC and non-refractory PM are detected with the laser engaged, but only non-refractory PM is detected when the laser is disengaged. Since the collection efficiency is increased (see section 3.1.2.1) by the use of two vaporizers rather than one, the slope of the correlation is normally above one. Ions which fall significantly above the general slope, as for example CO_2^+ in Figure 15, have contributions from rBC.

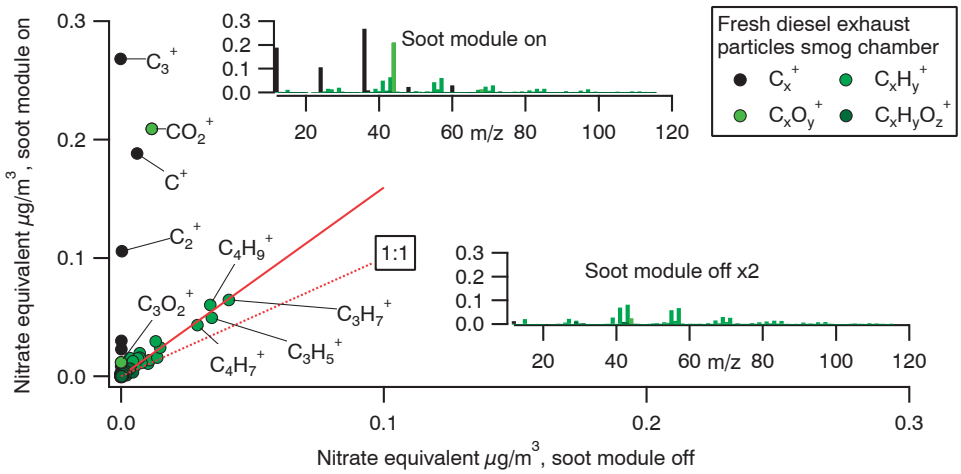

Fig 15. Black carbon heteroatoms (O) identified in diesel exhaust particles. Figure 2A in Article V.

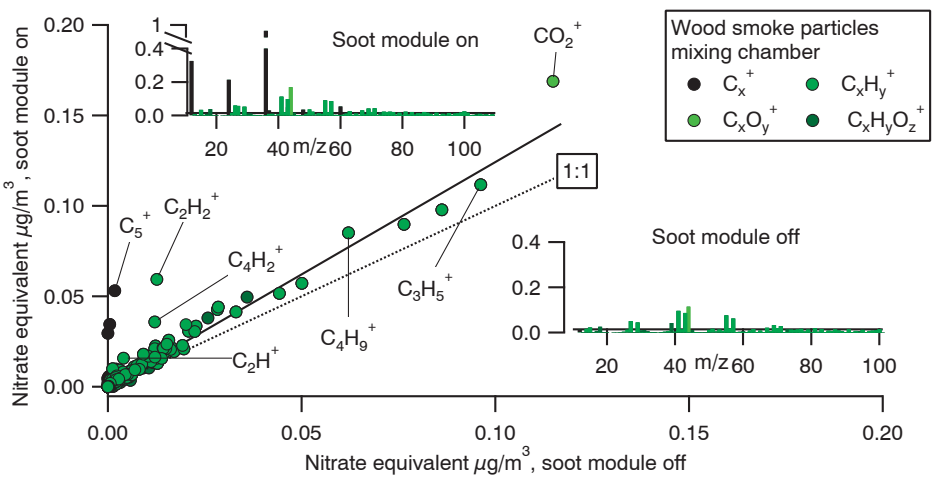

Figure 16. Black carbon heteroatoms (H and O) identified in wood smoke emitted at high burn rate.

While signal form refractory oxygen containing material ($rC_xO_y^+$) has so far been ubiquitous in all SP-AMS spectra of concentrated soot samples I have seen (wood-stoves, diesel engine exhaust, near traffic ambient air, as well as various burner soots, and commercially available samples), clear signals from refractory hydrogen containing material ($rC_xH_y^+$) are rarer. $rC_xH_y^+$ is expected to be more abundant in less mature soot, where the graphitization process has been interrupted (e.g. by quenching of flames by stove surfaces) or combustion temperatures and/or pressures are lower. Even when present, these signals are typically weaker than $rC_xO_y^+$ signals. In wood smoke for instance, it seems the main $rC_xH_y^+$ ion; $rC_2H_2^+$ is (as a rule of thumb) about as abundant as C_5^+, while CO^+; the main $rC_xO_y^+$ ion, is about as abundant as C_3^+ (i.e., typically an order of magnitude more abundant).

Although the scatter plot analysis is complicated by the differences in fragmentation patterns between the two vaporizers[81] these differences tend to reduce the apparent heteroatom content rather than increase it. The softer laser vaporization favors formation of larger ions, not the small ions identified as originating from rBC constituents. Furthermore, a constraint can be put on this issue (the difference in fragmentation patterns) by considering that the possible positive offsets from the general slope (which might be misinterpreted as BC heteroatoms) can be gauged from the scatter of the other ions. Fragmentation-induced differences will give both positive and negative offsets. Finally, for ions that are virtually absent in the spectrum when the laser vaporizer is disengaged, but have significant intensities when it is engaged (as $C_3O_2^+$ in Figure 15 above), the offset is unlikely to rise from fragmentation differences.

Another possible caveat is the temporal variability in the PM studied. In the ambient case (Article V) this caveat was mitigated by using an extended dataset (that way this effect will average out), while the wood smoke plot above (Figure 16) the issue was resolved by the use of batch-wise injection into a large mixing volume (see section 4.1.2 and Article II).

Quantifying the abundances of black carbon heteroatoms (and arguably the main point of the AMS technique is the possibility of quantification!) has proved challenging as there is a large instrument-to-instrument variability in sensitivity, and due to the lack of a suitable reference method. As there is good repeatability of qualitative comparisons across instruments ("sample X contains N times more oxygen than sample Y") and over time for one instrument and one sample, I believe we can and will resolve this issue with time.

5. Summary and conclusions

I have deployed a Soot-Particle Aerosol Mass Spectrometer (obviously there was auxiliary instrumentation, and many colleagues were involved!) in laboratory and field campaigns, and measured the chemical composition and microphysical properties of PM_1. My overall goal was to elucidate the emission and atmospheric transformation of soot particles. The studies were focused on emissions from wood stoves and light-duty vehicles. These are the main conclusions drawn from the research presented in this thesis:

Particulate PAH emission from wood stoves is highly dependent on combustion intensity. Some emissions occur shortly after fuel addition, which are difficult to avoid. Later in the combustion cycle, further emissions will be controlled by the combustion intensity. More intense combustion causes higher emissions. High combustion intensity is favored by dry fuel, high fuel addition rates, and small logs. Furthermore, emissions of SOA precursors and light-absorbing, climate warming carbonaceous particulates are also elevated under excessively intense combustion. The same is true for benzene (a carcinogen) and methane (a potent green-house gas). Consequently, it would be advantageous for both air quality and the mitigation of anthropogenic climate forcing if excessively intense wood combustion was avoided.

Well insulated biomass combustion appliances, such as modern wood stoves, can produce nearly black PM. The absorption Ångström exponents observed were closer to literature values for diesel exhaust than wood smoke. This means that source attribution efforts based on Absorption Ångström exponents will misattribute such emissions. Intense photochemical processing did little to change the measured optical properties of the PM.

Gasoline exhaust readily forms secondary PM. The secondary PM formed in the smog chamber outweighed primary PM emissions by one to three orders of magnitude. About half of the material formed was organic (SOA). The remainder was dominated by ammonium nitrate. Approximately half of the SOA derived from gasoline exhaust appears to have originated from C6-C9 aromatics, which are the main species implicated in the literature.

Diesel exhaust particles exhibit progressively increased hygroscopicity when photochemically aged together with light aromatic compounds in the laboratory. The fresh exhaust particles are hydrophobic. As UV light is supplied, a rapid (in less than five minutes) transformation occurs, and the particles become slightly hydrophilic,

and cloud condensation nuclei (CCN) activity begins at high supersaturations. With further photochemical processing, the particles' hydrophilicity increases monotonically, due to the condensation of secondary organic aerosol (SOA). The particles' ability to act as cloud condensation nuclei can be accurately modelled assuming constant SOA properties, except during the early phases of ageing (where the SOA constitutes less than ~10% of the particle mass). In this early stage of the ageing, the measured cloud condensation nuclei fraction is below the modelled one, possibly due to intrinsically different SOA.

As diesel exhaust particles become coated with SOA, their shapes are altered. This is partly due to the filling of open structures, and partly to restructuring of the soot core. The latter is an irreversible process which occurs predominantly in the later stages of ageing when the particles are dominated by SOA. When the ageing particles are exposed to humid (subsaturated) air, the restructuring is accelerated due to the water uptake of the SOA.

The ambient observations, which were made in wintertime Copenhagen and environs showed rapid and extensive transformation of diesel exhaust particles. In a few hours, the particles had grown into the accumulation mode, despite limited photochemistry. This was mainly due to the coupled addition of ammonium nitrate, and liquid water to the particles.

Black carbon, which is emitted by a range of processes where carbonaceous materials combust is not pure carbon. Even discounting the organic components (of which there always seems to be some judging from the mass spectra), there are still heteroatoms present in the BC particles. Heteroatoms in this context means "not carbon" atoms: oxygen and hydrogen.

6. Outlook

Further investigations of BC heteroatoms are warranted. BC volatilization in inert atmospheres can help elucidate the heteroatoms. Presumably, the surface oxides decompose at elevated temperatures (hotter than the 600 °C normally used in AMS vaporization). Burner soot data already acquired should be used to test the hypothesis that the refractory hydrogen originates from less mature BC components. The connection between refractory hydrogen and absorption Ångström exponents should be investigated. Comparison with in-situ X-ray Photoelecton Spectroscopy could show which functional groups contain the heteroatoms.

It is important to understand the instrument-to-instrument variability in BC heteroatom sensitivity. Ion source tuning and laser vaporizer power seems likely candidates to explain the variability. Another feature that would be interesting to investigate during such experiments (varying tuning and power) is the difference in response towards the vaporizers, normally folded into the ionization efficiencies of Regal Black and ammonium nitrate.

Future measurements on systems that feature rapid transients, such as street canyons, as well as wood smoke emissions, should be performed at 1 Hz sampling frequency (or faster depending on the sampling lines).

Acknowledgements

In 2008, I was introduced to the field of aerosol science by Anders Gudmundsson, to whom I am very grateful. (I contacted Prof. S. and he delegated, but in the long run, was not spared.) Since then I have made many new acquaintances, none of which I regret. I wonder which other occupation besides hermit where one can last seven years without a single unpleasant encounter!

To my advisors during these doctoral studies; Erik Swietlicki and Joakim Pagels: you make a good team! Your enthusiasm and know-how have been, and continue to be, a driving force. There are many areas of the physical sciences which fascinate me. It is your guidance that has channeled this fascination into aerosols in general and soot particles especially. I am very much looking forward to continuing what we have begun. Having spent so much time figuring out how the device works, I'm looking forward to now using that knowledge. Also, let's see what tomorrow brings in terms of instrumentation. To Erik I am thankful for his ability to put things into perspective. Joakim is acknowledged for his extraordinary help with finalizing this thesis.

Thanks are due to Erik Nordin and Partik Nilsson who have been a part of my aerosol adventure almost from the start. Patrik has been my go-to person for hands-on assistance with the aerosols, without his expertise I do not know what I would have done. With the range of exotic particles we have put into one AMS we may possibly hold a record of some sort. To Erik I am grateful for good cooperation during and after the wood stove campaigns, good times in Umeå and abroad, and for helping me navigate many non-science aspects of our work, where I would have been hopelessly lost without his assistance. Also for having the good taste to celebrate his birthdays in coordination with the International Aerosol Conference.

I am grateful also to Pontus Roldin and Emilie Hermansson: the ADCHEM team. I have learnt a lot from talking to both of you and we have a lot to gain from coordinating our efforts. Thanks also to Emilie for being an excellent office mate.

Thanks to Cerina Wittbom, Moa Sporre, Erik Ahlberg, Birgitta Svenningsson, Staffan Sjögren and Jenny Rissler for sharing your expertise when I needed it.

Thanks Christina Isaxon, Christian Svensson, Adam Kristensson, Jakob Löndahl, and Aneta Wierzbicka for interesting discussions.

Eileen Deaner, you have done an excellent job helping me improve my texts. (Anything with, unusual punctuation is likely; a last minute addition.)

Thanks to Anneli Nilsson Ahlm and Karin Öhrvik for endless administrative support. My memory can apparently a bit selective, and you have shown an impressive politeness answering what I suspect were the same questions, again and again!

Christoffer Boman, Robin Nyström, Robert Lindgren, Johan Martinsson, Ingeborg Elbæk Nielsen, Jacob Klenø Nøjgaard and Vilhelm Malmborg are acknowledged for good work with wood smoke.

Thanks Ågot Watne, Xiangyu Pei, Mattias Hallquist and the rest of the Gothenburg group I have had the pleasure of interacting with.

I thank Sandra Török and Per-Erik Bengtsson for the exciting cooperation with the burner soot. Very much looking forward to seeing where it leads.

I thank Amewu Mensah, Joel Corbin and Sanna Saarikoski for a very rewarding cooperation. I learnt a lot in Zurich, and from the discussions that followed. The data-set collected is one of my favorite treasures. We have a unique opportunity there, if time can be found somehow.

The folks at Aerodyne have been very helpful, especially Ed Fortner, Manjula Canagaratna and Tim Onasch. Doug Worsnop deserves thanks also for sharing his infinite wisdom.

Donna Sueper is acknowledged for excellent support.

I also want to thank Aerosol group at Lund University for being a good work environment. And the AMS users group: those meetings have been extremely rewarding. The one in Busan was the best meeting ever.

Finacial support from the Swedish Research Council FORMAS (projects 2009-615, 2010-1678, 2011-732, 2013-1023) and the Swedish Research Council VR (projects 2010-4683 and 2013-5021) is acknowledged.

The field experiments at were carried out with the support of the European Seventh Framework Program, ACTRIS (EU INFRA-2010-1.1.16-262254), Aerosols, Clouds, and Trace gases Research Infra Structure Network; and the Swedish Strategic Research Program MERGE, Modeling the Regional and Global Earth System; and the Lund Centre for studies of Carbon Cycle and Climate Interaction, LUCCI; and the Nordic Council of Ministers for the Nordic Top-level Research initiative CRAICC: Cryosphere–Atmosphere Interactions In a Changing Arctic Climate.

The biomass combustion emission research was carried out within the ERA-NET project BIOHEALTH and the FORTE-centre METALUND.

Finally I give thanks to my family, especially my parents and bonus parents.

References

1. Petzold, A.; Ogren, J. A.; Fiebig, M.; Laj, P.; Li, S. M.; Baltensperger, U.; Holzer-Popp, T.; Kinne, S.; Pappalardo, G.; Sugimoto, N.; Wehrli, C.; Wiedensohler, A.; Zhang, X. Y., Recommendations for reporting "black carbon" measurements. *Atmos Chem Phys* **2013,** *13*, (16), 8365-8379.
2. www.who.int/mediacentre/news/releases/2014/air-pollution/en/ (accessed 2015-05-03)
3. Boucher, O.; Randall, D.; Artaxo, P.; Bretherton, C.; Feingold, G.; Forster, P.; Kerminen, V.; Kondo, Y.; Liao, H.; Lohmann, U., Climate change 2013: the physical science basis. *Clouds and Aerosols. Contribution of Working Group I to the 5th assessment report of the intergovernmental panel on climate change, Cambridge University Press, Cambridge, United Kingdom and New York, NY, USA* **2013**.
4. Kandas, A. W.; Senel, I. G.; Levendis, Y.; Sarofim, A. F., Soot surface area evolution during air oxidation as evaluated by small angle X-ray scattering and CO2 adsorption. *Carbon* **2005,** *43*, (2), 241-251.
5. Jayne, J. T.; Leard, D. C.; Zhang, X. F.; Davidovits, P.; Smith, K. A.; Kolb, C. E.; Worsnop, D. R., Development of an aerosol mass spectrometer for size and composition analysis of submicron particles. *Aerosol Sci Tech* **2000,** *33*, (1-2), 49-70.
6. Canagaratna, M. R.; Jayne, J. T.; Jimenez, J. L.; Allan, J. D.; Alfarra, M. R.; Zhang, Q.; Onasch, T. B.; Drewnick, F.; Coe, H.; Middlebrook, A.; Delia, A.; Williams, L. R.; Trimborn, A. M.; Northway, M. J.; DeCarlo, P. F.; Kolb, C. E.; Davidovits, P.; Worsnop, D. R., Chemical and microphysical characterization of ambient aerosols with the aerodyne aerosol mass spectrometer. *Mass Spectrom Rev* **2007,** *26*, (2), 185-222.
7. Jimenez, J. L.; Canagaratna, M. R.; Donahue, N. M.; Prevot, A. S. H.; Zhang, Q.; Kroll, J. H.; DeCarlo, P. F.; Allan, J. D.; Coe, H.; Ng, N. L.; Aiken, A. C.; Docherty, K. S.; Ulbrich, I. M.; Grieshop, A. P.; Robinson, A. L.; Duplissy, J.; Smith, J. D.; Wilson, K. R.; Lanz, V. A.; Hueglin, C.; Sun, Y. L.; Tian, J.; Laaksonen, A.; Raatikainen, T.; Rautiainen, J.; Vaattovaara, P.; Ehn, M.; Kulmala, M.; Tomlinson, J. M.; Collins, D. R.; Cubison, M. J.; Dunlea, E. J.; Huffman, J. A.; Onasch, T. B.; Alfarra, M. R.; Williams, P. I.; Bower, K.; Kondo, Y.; Schneider, J.; Drewnick, F.; Borrmann, S.; Weimer, S.; Demerjian, K.; Salcedo, D.; Cottrell, L.; Griffin, R.; Takami, A.; Miyoshi, T.; Hatakeyama, S.; Shimono, A.; Sun, J. Y.; Zhang, Y. M.; Dzepina, K.; Kimmel, J. R.; Sueper, D.; Jayne, J. T.; Herndon, S. C.; Trimborn, A. M.; Williams, L. R.; Wood, E. C.; Middlebrook, A. M.; Kolb, C. E.; Baltensperger, U.; Worsnop, D. R., Evolution of Organic Aerosols in the Atmosphere. *Science* **2009,** *326*, (5959), 1525-1529.
8. Onasch, T. B.; Trimborn, A.; Fortner, E. C.; Jayne, J. T.; Kok, G. L.; Williams, L. R.; Davidovits, P.; Worsnop, D. R., Soot particle aerosol mass spectrometer: development, validation, and initial application. *Aerosol Sci Tech* **2012,** *46*, (7), 804-817.

9. IPCC, *Climate Change 2013: The Physical Science Basis. Contribution of Working Group I to the Fifth Assessment Report of the Intergovernmental Panel on Climate Change*. Cambridge University Press: Cambridge, United Kingdom and New York, NY, USA, 2013; p 1535.
10. Keeling, C. D., The Concentration and Isotopic Abundances of Carbon Dioxide in the Atmosphere. *Tellus* **1960,** *12*, (2), 200-203.
11. Stocker, T. F.; Qin, D.; Plattner, G.-K.; Alexander, L. V.; Allen, S. K.; Bindoff, N. L.; Bréon, F.-M.; Church, J. A.; Cubasch, U.; Emori, S.; Forster, P.; Friedlingstein, P.; Gillett, N.; Gregory, J. M.; Hartmann, D. L.; Jansen, E.; Kirtman, B.; Knutti, R.; Krishna Kumar, K.; Lemke, P.; Marotzke, J.; Masson-Delmotte, V.; Meehl, G. A.; Mokhov, I. I.; Piao, S.; Ramaswamy, V.; Randall, D.; Rhein, M.; Rojas, M.; Sabine, C.; Shindell, D.; Talley, L. D.; Vaughan, D. G.; Xie, S.-P., Technical Summary. In *Climate Change 2013: The Physical Science Basis. Contribution of Working Group I to the Fifth Assessment Report of the Intergovernmental Panel on Climate Change*, Stocker, T. F.; Qin, D.; Plattner, G.-K.; Tignor, M.; Allen, S. K.; Boschung, J.; Nauels, A.; Xia, Y.; Bex, V.; Midgley, P. M., Eds. Cambridge University Press: Cambridge, United Kingdom and New York, NY, USA, 2013; pp 33–115.
12. Jacobson, M. Z., Strong radiative heating due to the mixing state of black carbon in atmospheric aerosols. *Nature* **2001,** *409*, (6821), 695-697.
13. Bond, T. C.; Doherty, S. J.; Fahey, D. W.; Forster, P. M.; Berntsen, T.; DeAngelo, B. J.; Flanner, M. G.; Ghan, S.; Karcher, B.; Koch, D.; Kinne, S.; Kondo, Y.; Quinn, P. K.; Sarofim, M. C.; Schultz, M. G.; Schulz, M.; Venkataraman, C.; Zhang, H.; Zhang, S.; Bellouin, N.; Guttikunda, S. K.; Hopke, P. K.; Jacobson, M. Z.; Kaiser, J. W.; Klimont, Z.; Lohmann, U.; Schwarz, J. P.; Shindell, D.; Storelvmo, T.; Warren, S. G.; Zender, C. S., Bounding the role of black carbon in the climate system: A scientific assessment. *J Geophys Res-Atmos* **2013,** *118*, (11), 5380-5552.
14. Rogelj, J.; Schaeffer, M.; Meinshausen, M.; Shindell, D. T.; Hare, W.; Klimont, Z.; Velders, G. J. M.; Amann, M.; Schellnhuber, H. J., Disentangling the effects of CO2 and short-lived climate forcer mitigation. *P Natl Acad Sci USA* **2014,** *111*, (46), 16325-16330.
15. Hallquist, M.; Wenger, J. C.; Baltensperger, U.; Rudich, Y.; Simpson, D.; Claeys, M.; Dommen, J.; Donahue, N. M.; George, C.; Goldstein, A. H.; Hamilton, J. F.; Herrmann, H.; Hoffmann, T.; Iinuma, Y.; Jang, M.; Jenkin, M. E.; Jimenez, J. L.; Kiendler-Scharr, A.; Maenhaut, W.; McFiggans, G.; Mentel, T. F.; Monod, A.; Prevot, A. S. H.; Seinfeld, J. H.; Surratt, J. D.; Szmigielski, R.; Wildt, J., The formation, properties and impact of secondary organic aerosol: current and emerging issues. *Atmos Chem Phys* **2009,** *9*, (14), 5155-5236.
16. Jathar, S. H.; Gordon, T. D.; Hennigan, C. J.; Pye, H. O. T.; Pouliot, G.; Adams, P. J.; Donahue, N. M.; Robinson, A. L., Unspeciated organic emissions from combustion sources and their influence on the secondary organic aerosol budget in the United States. *P Natl Acad Sci USA* **2014,** *111*, (29), 10473-10478.
17. Brook, R. D.; Rajagopalan, S.; Pope, C. A.; Brook, J. R.; Bhatnagar, A.; Diez-Roux, A. V.; Holguin, F.; Hong, Y. L.; Luepker, R. V.; Mittleman, M. A.; Peters, A.; Siscovick, D.; Smith, S. C.; Whitsel, L.; Kaufman, J. D.; Epidemiol, A. H. A. C.; Dis, C. K. C.; Metab, C. N. P. A., Particulate Matter Air Pollution and Cardiovascular Disease An Update to the Scientific Statement From the American Heart Association. *Circulation* **2010,** *121*, (21), 2331-2378.

18. Dockery, D. W.; Pope, C. A.; Xu, X. P.; Spengler, J. D.; Ware, J. H.; Fay, M. E.; Ferris, B. G.; Speizer, F. E., An Association between Air-Pollution and Mortality in 6 United-States Cities. *New Engl J Med* **1993,** *329*, (24), 1753-1759.
19. Heal, M. R.; Kumar, P.; Harrison, R. M., Particles, air quality, policy and health. *Chem Soc Rev* **2012,** *41*, (19), 6606-6630.
20. Gustafsson, M.; Forsberg, B.; Orru, H.; Åström, S.; Haben, T.; Sjöberg, K., Quantification of population exposure to NO2, PM2. 5 and PM10 and estimated health impacts in Sweden 2010. **2014**.
21. Janssen, N. A.; Gerlofs-Nijland, M. E.; Lanki, T.; Salonen, R. O.; Cassee, F.; Hoek, G.; Fischer, P.; Brunekreef, B.; Krzyzanowski, M., *Health effects of black carbon*. WHO Regional Office for Europe Copenhagen: 2012.
22. Air quality in Europe — 2014 report EEA Report No 5/2014. ISSN 1725-9177
23. http://www.who.int/indoorair/en/ (accessed 2015-05-03)
24. Costs of air pollution from European industrial facilities 2008–2012 EEA Technical report No 20/2014. ISSN 1725-2237
25. DeCarlo, P. F.; Kimmel, J. R.; Trimborn, A.; Northway, M. J.; Jayne, J. T.; Aiken, A. C.; Gonin, M.; Fuhrer, K.; Horvath, T.; Docherty, K. S.; Worsnop, D. R.; Jimenez, J. L., Field-deployable, high-resolution, time-of-flight aerosol mass spectrometer. *Anal Chem* **2006,** *78*, (24), 8281-8289.
26. Stephens, M.; Turner, N.; Sandberg, J., Particle identification by laser-induced incandescence in a solid-state laser cavity. *Applied optics* **2003,** *42*, (19), 3726-3736.
27. Liu, P.; Ziemann, P. J.; Kittelson, D. B.; McMurry, P. H., Generating Particle Beams of Controlled Dimensions and Divergence: II. Experimental Evaluation of Particle Motion in Aerodynamic Lenses and Nozzle Expansions. *Aerosol Sci Tech* **1995,** *22*, (3), 314-324.
28. Lanz, V. A.; Alfarra, M. R.; Baltensperger, U.; Buchmann, B.; Hueglin, C.; Prevot, A. S. H., Source apportionment of submicron organic aerosols at an urban site by factor analytical modelling of aerosol mass spectra. *Atmos Chem Phys* **2007,** *7*, (6), 1503-1522.
29. Kroll, J. H.; Donahue, N. M.; Jimenez, J. L.; Kessler, S. H.; Canagaratna, M. R.; Wilson, K. R.; Altieri, K. E.; Mazzoleni, L. R.; Wozniak, A. S.; Bluhm, H., Carbon oxidation state as a metric for describing the chemistry of atmospheric organic aerosol. *Nature Chemistry* **2011,** *3*, (2), 133-139.
30. Ovadnevaite, J.; Ceburnis, D.; Canagaratna, M.; Berresheim, H.; Bialek, J.; Martucci, G.; Worsnop, D. R.; O'Dowd, C., On the effect of wind speed on submicron sea salt mass concentrations and source fluxes. *Journal of Geophysical Research: Atmospheres (1984–2012)* **2012,** *117*, (D16).
31. Salcedo, D.; Onasch, T.; Aiken, A.; Williams, L.; Foy, B. d.; Cubison, M.; Worsnop, D.; Molina, L.; Jimenez, J., Determination of particulate lead using aerosol mass spectrometry: MILAGRO/MCMA-2006 observations. *Atmos Chem Phys* **2010,** *10*, (12), 5371-5389.
32. Salcedo, D.; Laskin, A.; Shutthanandan, V.; Jimenez, J.-L., Feasibility of the detection of trace elements in particulate matter using online high-resolution aerosol mass spectrometry. *Aerosol Sci Tech* **2012,** *46*, (11), 1187-1200.
33. Nilsson, P. T.; Isaxon, C.; Eriksson, A. C.; Messing, M. E.; Ludvigsson, L.; Rissler, J.; Hedmer, M.; Tinnerberg, H.; Gudmundsson, A.; Deppert, K., Nano-objects emitted during

maintenance of common particle generators: direct chemical characterization with aerosol mass spectrometry and implications for risk assessments. *J Nanopart Res* **2013,** *15*, (11), 1-16.
34. http://cires1.colorado.edu/jimenez-group/wiki/index.php/Field_ToF-AMS_Operation Accessed 2015-05-03
35. Huffman, J. A.; Jayne, J. T.; Drewnick, F.; Aiken, A. C.; Onasch, T.; Worsnop, D. R.; Jimenez, J. L., Design, modeling, optimization, and experimental tests of a particle beam width probe for the aerodyne aerosol mass spectrometer. *Aerosol Sci Tech* **2005,** *39*, (12), 1143-1163.
36. Zhang, X.; Smith, K. A.; Worsnop, D. R.; Jimenez, J. L.; Jayne, J. T.; Kolb, C. E.; Morris, J.; Davidovits, P., Numerical characterization of particle beam collimation: Part II integrated aerodynamic-lens–nozzle system. *Aerosol Sci Tech* **2004,** *38*, (6), 619-638.
37. Willis, M.; Lee, A.; Onasch, T.; Fortner, E.; Williams, L.; Lambe, A.; Worsnop, D.; Abbatt, J., Collection efficiency of the Soot-Particle Aerosol Mass Spectrometer (SP-AMS) for internally mixed particulate black carbon. *Atmos Meas Tech* **2014,** *7*, (12), 4507-4516.
38. Matthew, B. M.; Middlebrook, A. M.; Onasch, T. B., Collection efficiencies in an Aerodyne Aerosol Mass Spectrometer as a function of particle phase for laboratory generated aerosols. *Aerosol Sci Tech* **2008,** *42*, (11), 884-898.
39. Middlebrook, A. M.; Bahreini, R.; Jimenez, J. L.; Canagaratna, M. R., Evaluation of composition-dependent collection efficiencies for the aerodyne aerosol mass spectrometer using field data. *Aerosol Sci Tech* **2012,** *46*, (3), 258-271.
40. DeCarlo, P. F.; Slowik, J. G.; Worsnop, D. R.; Davidovits, P.; Jimenez, J. L., Particle morphology and density characterization by combined mobility and aerodynamic diameter measurements. Part 1: theory. *Aerosol Sci Tech* **2004,** *38*, (12), 1185-1205.
41. Allan, J. D.; Jimenez, J. L.; Williams, P. I.; Alfarra, M. R.; Bower, K. N.; Jayne, J. T.; Coe, H.; Worsnop, D. R., Quantitative sampling using an Aerodyne aerosol mass spectrometer 1. Techniques of data interpretation and error analysis. *Journal of Geophysical Research: Atmospheres (1984–2012)* **2003,** *108*, (D3).
42. http://cires1.colorado.edu/jimenezgroup/ToFAMSResources/ToFSoftware/index.html (accessed 2015-05-03)
43. Allan, J. D.; Delia, A. E.; Coe, H.; Bower, K. N.; Alfarra, M. R.; Jimenez, J. L.; Middlebrook, A. M.; Drewnick, F.; Onasch, T. B.; Canagaratna, M. R., A generalised method for the extraction of chemically resolved mass spectra from Aerodyne aerosol mass spectrometer data. *J Aerosol Sci* **2004,** *35*, (7), 909-922.
44. Yli-Juuti, T.; Zardini, A. A.; Eriksson, A. C.; Hansen, A. M. K.; Pagels, J. H.; Swietlicki, E.; Svenningsson, B.; Glasius, M.; Worsnop, D. R.; Riipinen, I.; Bilde, M., Volatility of Organic Aerosol: Evaporation of Ammonium Sulfate/Succinic Acid Aqueous Solution Droplets. *Environ Sci Technol* **2013,** *47*, (21), 12123-12130.
45. Roldin, P.; Eriksson, A. C.; Nordin, E. Z.; Hermansson, E.; Mogensen, D.; Rusanen, A.; Boy, M.; Swietlicki, E.; Svenningsson, B.; Zelenyuk, A.; Pagels, J., Modelling non-equilibrium secondary organic aerosol formation and evaporation with the aerosol dynamics, gas- and particle-phase chemistry kinetic multilayer model ADCHAM. *Atmos Chem Phys* **2014,** *14*, (15), 7953-7993.

46. Zhang, X.; Cappa, C. D.; Jathar, S. H.; Mcvay, R. C.; Ensberg, J. J.; Kleeman, M. J.; Seinfeld, J. H., Influence of vapor wall loss in laboratory chambers on yields of secondary organic aerosol. *P Natl Acad Sci USA* **2014,** *111*, (16), 5802-5807.
47. Kang, E.; Root, M. J.; Toohey, D. W.; Brune, W. H., Introducing the concept of Potential Aerosol Mass (PAM). *Atmos Chem Phys* **2007,** *7*, (22), 5727-5744.
48. Bruns, E.; El Haddad, I.; Keller, A.; Klein, F.; Kumar, N.; Pieber, S.; Corbin, J.; Slowik, J.; Brune, W.; Baltensperger, U., Inter-comparison of laboratory smog chamber and flow reactor systems on organic aerosol yield and composition. *Atmospheric Measurement Techniques Discussions* **2015,** *8*, (1), 309-352.
49. Ehara, K.; Hagwood, C.; Coakley, K. J., Novel method to classify aerosol particles according to their mass-to-charge ratio - Aerosol particle mass analyser. *J Aerosol Sci* **1996,** *27*, (2), 217-234.
50. McMurry, P. H.; Wang, X.; Park, K.; Ehara, K., The relationship between mass and mobility for atmospheric particles: A new technique for measuring particle density. *Aerosol Sci Tech* **2002,** *36*, (2), 227-238.
51. Drinovec, L.; Močnik, G.; Zotter, P.; Prévôt, A.; Ruckstuhl, C.; Coz, E.; Rupakheti, M.; Sciare, J.; Müller, T.; Wiedensohler, A., The" dual-spot" Aethalometer: an improved measurement of aerosol black carbon with real-time loading compensation. *Atmospheric Measurement Techniques Discussions* **2014,** *7*, (9), 10179-10220.
52. Pettersson, E.; Boman, C.; Westerholm, R.; Bostrom, D.; Nordin, A., Stove performance and emission characteristics in residential wood log and pellet combustion, part 2: wood stove. *Energ Fuel* **2011,** *25*, 315-323.
53. Chen, Y.; Bond, T. C., Light absorption by organic carbon from wood combustion. *Atmos Chem Phys* **2010,** *10*, (4), 1773-1787.
54. Laskin, A.; Laskin, J.; Nizkorodov, S. A., Chemistry of Atmospheric Brown Carbon. *Chemical Reviews* **2015**.
55. Saleh, R.; Robinson, E. S.; Tkacik, D. S.; Ahern, A. T.; Liu, S.; Aiken, A. C.; Sullivan, R. C.; Presto, A. A.; Dubey, M. K.; Yokelson, R. J.; Donahue, N. M.; Robinson, A. L., Brownness of organics in aerosols from biomass burning linked to their black carbon content. *Nat Geosci* **2014,** *7*, (9), 647-650.
56. Sato, K.; Takami, A.; Kato, Y.; Seta, T.; Fujitani, Y.; Hikida, T.; Shimono, A.; Imamura, T., AMS and LC/MS analyses of SOA from the photooxidation of benzene and 1,3,5-trimethylbenzene in the presence of NOx: effects of chemical structure on SOA aging. *Atmos Chem Phys* **2012,** *12*, (10), 4667-4682.
57. Lee, H. J.; Aiona, P. K.; Laskin, A.; Laskin, J.; Nizkorodov, S. A., Effect of Solar Radiation on the Optical Properties and Molecular Composition of Laboratory Proxies of Atmospheric Brown Carbon. *Environ Sci Technol* **2014,** *48*, (17), 10217-10226.
58. Jacobson, M. Z., Studying the effects of aerosols on vertical photolysis rate coefficient and temperature profiles over an urban airshed. *J Geophys Res-Atmos* **1998,** *103*, (D9), 10593-10604.
59. Sandradewi, J.; Prevot, A. S. H.; Szidat, S.; Perron, N.; Alfarra, M. R.; Lanz, V. A.; Weingartner, E.; Baltensperger, U., Using aerosol light absorption measurements for the quantitative determination of wood burning and traffic emission contributions to particulate matter. *Environ Sci Technol* **2008,** *42*, (9), 3316-3323.

60. Bond, T. C.; Covert, D. S.; Kramlich, J. C.; Larson, T. V.; Charlson, R. J., Primary particle emissions from residential coal burning: Optical properties and size distributions. *J Geophys Res-Atmos* **2002,** *107*, (D21).
61. Kimmel, J. R.; Farmer, D. K.; Cubison, M. J.; Sueper, D.; Tanner, C.; Nemitz, E.; Worsnop, D. R.; Gonin, M.; Jimenez, J. L., Real-time aerosol mass spectrometry with millisecond resolution. *Int J Mass Spectrom* **2011,** *303*, (1), 15-26.
62. Paloposki, T.; Saastamoinen, J.; Klobut, K.; Tuomaala, P., Analysis of wood firing in stoves by the oxygen consumption method and the carbon dioxide generation method. *Biomass and Bioenergy* **2012**.
63. Farmer, D. K.; Matsunaga, A.; Docherty, K. S.; Surratt, J. D.; Seinfeld, J. H.; Ziemann, P. J.; Jimenez, J. L., Response of an aerosol mass spectrometer to organonitrates and organosulfates and implications for atmospheric chemistry. *P Natl Acad Sci USA* **2010,** *107*, (15), 6670-6675.
64. Jonsson, Å. M.; Hallquist, M.; Saathoff, H., Volatility of secondary organic aerosols from the ozone initiated oxidation of α-pinene and limonene. *Journal of Aerosol Science* **2007,** *38*, (8), 843-852.
65. Salo, K.; Westerlund, J.; Andersson, P. U.; Nielsen, C.; D'Anna, B.; Hallquist, M., Thermal Characterization of Aminium Nitrate Nanoparticles. *J Phys Chem A* **2011,** *115*, (42), 11671-11677.
66. Huffman, J. A.; Docherty, K. S.; Aiken, A. C.; Cubison, M. J.; Ulbrich, I. M.; DeCarlo, P. F.; Sueper, D.; Jayne, J. T.; Worsnop, D. R.; Ziemann, P. J.; Jimenez, J. L., Chemically-resolved aerosol volatility measurements from two megacity field studies. *Atmos Chem Phys* **2009,** *9*, (18), 7161-7182.
67. Kohler, H., The nucleus in and the growth of hygroscopic droplets. *T Faraday Soc* **1936,** *32*, (2), 1152-1161.
68. Petters, M. D.; Kreidenweis, S. M., A single parameter representation of hygroscopic growth and cloud condensation nucleus activity. *Atmos Chem Phys* **2007,** *7*, (8), 1961-1971.
69. Aubin, D. G.; Abbatt, J. P. D., Interaction of NO2 with hydrocarbon soot: Focus on HONO yield, surface modification, and mechanism. *J Phys Chem A* **2007,** *111*, (28), 6263-6273.
70. Monge, M. E.; D'Anna, B.; Mazri, L.; Giroir-Fendler, A.; Ammann, M.; Donaldson, D. J.; George, C., Light changes the atmospheric reactivity of soot. *Proc Natl Acad Sci U S A* **2010,** *107*, (15), 6605-9.
71. Schnitzler, E. G.; Dutt, A.; Charbonneau, A. M.; Olfert, J. S.; Jager, W., Soot Aggregate Restructuring Due to Coatings of Secondary Organic Aerosol Derived from Aromatic Precursors. *Environ Sci Technol* **2014,** *48*, (24), 14309-14316.
72. Rissler, J.; Nordin, E. Z.; Eriksson, A. C.; Nilsson, P. T.; Frosch, M.; Sporre, M. K.; Wierzbicka, A.; Svenningsson, B.; Londahl, J.; Messing, M. E.; Sjogren, S.; Hemmingsen, J. G.; Loft, S.; Pagels, J. H.; Swietlicki, E., Effective density and mixing state of aerosol particles in a near-traffic urban environment. *Environ Sci Technol* **2014,** *48*, (11), 6300-8.
73. www.actris.net (accessed 2015-05-03)
74. Kristensson, A.; Dal Maso, M.; Swietlicki, E.; Hussein, T.; Zhou, J.; KERMINEN, V. M.; Kulmala, M., Characterization of new particle formation events at a background site in Southern Sweden: relation to air mass history. *Tellus B* **2008,** *60*, (3), 330-344.

75. Beekmann, M.; Prévôt, A. S. H.; Drewnick, F.; Sciare, J.; Pandis, S. N.; Denier van der Gon, H. A. C.; Crippa, M.; Freutel, F.; Poulain, L.; Ghersi, V.; Rodriguez, E.; Beirle, S.; Zotter, P.; von der Weiden-Reinmüller, S. L.; Bressi, M.; Fountoukis, C.; Petetin, H.; Szidat, S.; Schneider, J.; Rosso, A.; El Haddad, I.; Megaritis, A.; Zhang, Q. J.; Michoud, V.; Slowik, J. G.; Moukhtar, S.; Kolmonen, P.; Stohl, A.; Eckhardt, S.; Borbon, A.; Gros, V.; Marchand, N.; Jaffrezo, J. L.; Schwarzenboeck, A.; Colomb, A.; Wiedensohler, A.; Borrmann, S.; Lawrence, M.; Baklanov, A.; Baltensperger, U., In-situ, satellite measurement and model evidence for a~dominant regional contribution to fine particulate matter levels in the Paris Megacity. *Atmos. Chem. Phys. Discuss.* **2015,** *15*, (6), 8647-8686.
76. Fierce, L.; Riemer, N.; Bond, T. C., Explaining variance in black carbon's aging timescale. *Atmos. Chem. Phys.* **2015,** *15*, (6), 3173-3191.
77. Hermansson, E.; Roldin, P.; Rusanen, A.; Mogensen, D.; Kivekäs, N.; Väänänen, R.; Boy, M.; Swietlicki, E., Biogenic SOA formation through gas-phase oxidation and gas-to-particle partitioning–a comparison between process models of varying complexity. *Atmos Chem Phys* **2014,** *14*, (21), 11853-11869.
78. Zhang, R.; Khalizov, A. F.; Pagels, J.; Zhang, D.; Xue, H.; McMurry, P. H., Variability in morphology, hygroscopicity, and optical properties of soot aerosols during atmospheric processing. *Proceedings of the National Academy of Sciences* **2008,** *105*, (30), 10291-10296.
79. Cross, E. S.; Onasch, T. B.; Ahern, A.; Wrobel, W.; Slowik, J. G.; Olfert, J.; Lack, D. A.; Massoli, P.; Cappa, C. D.; Schwarz, J. P., Soot particle studies—instrument inter-comparison—project overview. *Aerosol Science and Technology* **2010,** *44*, (8), 592-611.
80. Crippa, M.; Canonaco, F.; Lanz, V. A.; Aijala, M.; Allan, J. D.; Carbone, S.; Capes, G.; Ceburnis, D.; Dall'Osto, M.; Day, D. A.; DeCarlo, P. F.; Ehn, M.; Eriksson, A.; Freney, E.; Ruiz, L. H.; Hillamo, R.; Jimenez, J. L.; Junninen, H.; Kiendler-Scharr, A.; Kortelainen, A. M.; Kulmala, M.; Laaksonen, A.; Mensah, A.; Mohr, C.; Nemitz, E.; O'Dowd, C.; Ovadnevaite, J.; Pandis, S. N.; Petaja, T.; Poulain, L.; Saarikoski, S.; Sellegri, K.; Swietlicki, E.; Tiitta, P.; Worsnop, D. R.; Baltensperger, U.; Prevot, A. S. H., Organic aerosol components derived from 25 AMS data sets across Europe using a consistent ME-2 based source apportionment approach. *Atmos Chem Phys* **2014,** *14*, (12), 6159-6176.
81. Canagaratna, M. R.; Massoli, P.; Browne, E. C.; Franklin, J. P.; Wilson, K. R.; Onasch, T. B.; Kirchstetter, T. W.; Fortner, E. C.; Kolb, C. E.; Jayne, J. T., Chemical Compositions of Black Carbon Particle Cores and Coatings via Soot Particle Aerosol Mass Spectrometry with Photoionization and Electron Ionization. *The Journal of Physical Chemistry A* **2014**.